DMRS-Based Uplink Channel Estimation for MU-MIMO Systems with Location-Specific SCSI Acquisition

Jiawei Zhuang, Hongwei Hou, *Graduate Student Member, IEEE*, Minjie Tang, Wenjin Wang, *Member, IEEE*, Shi Jin, *Fellow, IEEE*, Vincent K. N. Lau, *Fellow, IEEE*

***Abstract*—With the growing number of users in multi-user multiple-input multiple-output (MU-MIMO) systems, demodulation reference signals (DMRS) are efficiently multiplexed in the code domain via orthogonal cover codes (OCC) to ensure orthogonality and minimize pilot interference. In this paper, we investigate uplink DMRS-based channel estimation for MU-MIMO systems with Type II OCC pattern standardized in third generation partnership project (3GPP) Release 18, leveraging location-specific statistical channel state information (SCSI) to enhance performance. Specifically, we propose a SCSI-assisted Bayesian channel estimator (SA-BCE) based on the minimum mean square error criterion to suppress the pilot interference and noise, albeit at the cost of cubic computational complexity due to matrix inversions. To reduce this complexity while maintaining performance, we extend the scheme to a windowed version (SA-WBCE), which incorporates antenna-frequency domain windowing and beam-delay domain processing to exploit asymptotic sparsity and mitigate energy leakage in practical systems. To avoid the frequent real-time SCSI acquisition, we construct a grid-based location-specific SCSI database based on the principle of spatial consistency, and subsequently leverage the uplink received signals within each grid to extract the SCSI. Facilitated by the multilinear structure of wireless channels, we formulate the SCSI acquisition problem within each grid as a tensor decomposition problem, where the factor matrices are parameterized by the multi-path powers, delays, and angles. The computational complexity of SCSI acquisition can be significantly reduced by exploiting the Vandermonde structure of the factor matrices. Simulation results demonstrate that the proposed location-specific SCSI database construction method achieves high accuracy, while the SA-BCE and SA-WBCE significantly outperform state-of-the-art benchmarks in MU-MIMO systems.**

***Index Terms*—MU-MIMO, SCSI, channel estimation, tensor decomposition, demodulation reference signal**

I. Introduction

Manuscript received 8 June 2025; revised 10 October 2025; accepted 29 December 2025. This work was supported in part by the National Natural Science Foundation of China under Grant 62371122, in part by the Research Grants Council of Hong Kong through the Areas of Excellence Scheme under Grant AoE/E-101/23N, in part by the Research Grants Council of Hong Kong under Project CERG 16214122, and in part by the SNS JU project 6G-GOALS under the EU's Horizon programme Grant Agreement No. 101139232. This paper is an extended version of "A Bayesian Approach to Windowed DMRS Channel Estimation for Uplink MU-MIMO Systems" [1], which was presented at 2025 IEEE Globecom Workshops (GCWkshps) in Taipei, Taiwan. The associate editor coordinating the review of this manuscript and approving it for publication was Dr. Fang Fang. *(Corresponding author: Wenjin Wang.)*

Jiawei Zhuang, Hongwei Hou, and Wenjin Wang are with the National Mobile Communications Research Laboratory, Southeast University, Nanjing 210096, China, and also with Purple Mountain Laboratories, Nanjing 211100, China (e-mail: {jw-zhuang, hongweihou,wangwj}@seu.edu.cn).

Minjie Tang is with the Department of Communication Systems, EURECOM, France (e-mail: Minjie.Tang@eurecom.fr).

Shi Jin is with the National Mobile Communications Research Laboratory, Southeast University, Nanjing 210096, China (e-mail: jinshi@seu.edu.cn).

Vincent K. N. Lau is with the Department of Electronic and Computer Engineering, Hong Kong University of Science and Technology, Hong Kong 999077, China (e-mail: eeknlau@ust.hk).

DRIVEN by the growing demand for data-hungry applications such as broadband internet of things (IoT) [2] and extended reality (XR) [3], uplink-centric broadband communication (UCBC) [4] has emerged as a crucial service category in the era of forthcoming sixth-generation (6G) networks [5] [6]. To better understand this trend, it is instructive to examine the uplink demands of representative applications. Specifically, IoT applications demand support for a massive number of devices transmitting concurrent uplink traffic, while XR applications require high data rates, collectively resulting in an enormous uplink traffic volume. As a consequence, 6G networks must achieve at least a tenfold increase in uplink capacity to effectively support these data-intensive applications in the UCBC. To meet this requirement, multi-user multiple-input multiple-output (MU-MIMO) [7] [8] has emerged as a key technology for increasing uplink capacity in UCBC, by enabling concurrent transmissions from multiple users. As uplink traffic demand continues to escalate in UCBC scenarios, further expansion of the number of data streams becomes essential. In this regard, the number of orthogonal pilot ports increases from 12 to 24 in third generation partnership project (3GPP) Release 18 [9], enabling uplink transmission for up to 24 users.

However, the increase in orthogonal pilot ports aggravates the challenge of accurate channel state information (CSI) acquisition. Specifically, the CSI of multiple users is estimated via uplink demodulation reference signals (DMRS) [9], whose performance degrades as the number of users increases due to the inevitable overlap of DMRS on the same resource element (RE), thereby constraining the spectral efficiency of MU-MIMO systems. The improvement of DMRS-based channel estimation is thus indispensable for achieving reliable and efficient uplink MU-MIMO transmissions.

A. Prior Work

In MU-MIMO uplink transmission, orthogonal cover codes (OCC) are typically employed to enable code-domain multiplexing of DMRS from multiple users, resulting in their overlap on the same RE. Therefore, a critical step in uplink DMRS channel estimation is to separate the DMRS of different users through OCC decomposition. Based on the assumption that the channels remain unchanged over consecutive subcarriers, many works on uplink DMRS channel estimation leverage the orthogonality of different pilot ports to achieve OCC decomposition [10] [11]. However, this assumption breaks down in the presence of frequency-selective fading channel, compromising the orthogonality among different pilot ports and consequently introducing pilot interference. To address

this issue, the author in [12] proposed an minimum mean square error (MMSE) scheme for two-port DMRS channel estimation in New Radio systems, which exploits frequency-domain channel correlations to facilitate OCC decomposition.

However, the method in [12] assumes that statistical channel state information (SCSI) is perfectly known, which is unrealistic in practical systems. To this end, several SCSI acquisition approaches have been proposed in massive MIMO systems [13]–[19]. In [13] and [14], the instantaneous CSI (ICSI) is first estimated through pilot transmission, and SCSI is then derived by performing statistical calculations on the estimated ICSI. Expectation-maximization (EM) algorithm [20] provides another method for obtaining SCSI, where the ICSI and SCSI are iteratively estimated [15] [16] [17]. Some studies [18] [19] also proposed methods for acquiring SCSI without the need for ICSI. In [18], the authors employed multiple signal classification algorithms for SCSI acquisition, in which angles and delays are estimated from the received signals. The author in [19] proposed a novel approach for obtaining the beam-domain channel power matrices based on the received signal model and Kullback-Leibler divergence.

The aforementioned SCSI acquisition methods primarily rely on real-time received signals for SCSI estimation, which leads to large reference signal overhead and processing delay. Owing to the intrinsic relationship between SCSI and the wireless channel's scattering environment, a consistent mapping exists between user location and SCSI in stationary environments. This motivates the construction of location-specific SCSI database [21] [22], thereby converting the real-time estimation of SCSI into the problem of mapping construction. Toward this end, various location-specific SCSI database construction methods have been proposed in [23]–[25]. These approaches leverage error-free SCSI at specific locations to infer the location-specific SCSI over the entire region via MMSE-based spatial interpolation [23], subregional learning [24] and Laplacian pyramid–based image-to-image inpainting [25], respectively.

Current approaches to building location-specific SCSI databases [23]–[25] often rely on the idealized assumption of error-free SCSI samples, which rarely holds in practical deployment scenarios. This motivates the investigation of location-specific SCSI database construction methods that exploit noisy received signals at the base station (BS). However, the use of noisy received signals at the BS introduces new challenges. The received signal-to-noise ratio (SNR) at the BS is limited due to the constrained transmitted power of user equipment. In addition, the received signals exhibit a nonlinear relationship with the underlying SCSI parameters, such as the delay response vector [26]. To address these issues, the author in [27] employed Bayesian inference to suppress inter-cell interference and resolved the nonlinear mapping between received signals and SCSI parameters, paving the way for location-specific SCSI acquisition using the noisy BS received signals.

B. Motivation and Main Contributions

The state-of-the-art primarily exploits the orthogonality of OCC to enable OCC decomposition under the assumption of frequency flat-fading, which becomes invalid in propagation environments with significant delay spread. Meanwhile, efforts to enhance channel estimation via location-specific SCSI often rely on idealized, error-free channel samples, underscoring the need to incorporate noisy received signals for improved practical relevance. Moreover, as future communication systems scale in both antenna array size and bandwidth, constructing location-specific SCSI database becomes increasingly complex, necessitating the development of low-complexity solutions.

In this paper, we investigate the SCSI-assisted DMRS-based channel estimation in MU-MIMO systems and develop the corresponding location-specific SCSI database construction algorithm. The main contributions of this work are summarized as follows:

- By incorporating the Type II DMRS configuration in 3GPP Release 18, we develop the signal model for uplink DMRS-based channel estimation. The code-domain multiplexing of DMRS from multiple users on the same RE results in pilot interference, especially in frequency-selective fading channels. To mitigate such pilot interference, we formulate the uplink multi-user DMRS-based channel estimation problem based on the MMSE criterion, leveraging the statistical characteristics of the channel to effectively suppress noise and pilot interference.
- Building on the MMSE formulation, we propose a SCSI-assisted Bayesian channel estimator (SA-BCE) to achieve the DMRS-based channel estimation. Specifically, SA-BCE employs a frequency-domain MMSE estimator to mitigate the pilot interference, followed by an antenna-domain MMSE estimator to further suppress the noise. To reduce the computational complexity of SA-BCE, we shift from the antenna-frequency domain to the beam-delay domain and extend the scheme to windowed SA-BCE (SA-WBCE) to alleviate the energy leakage resulting from the finite number of subcarriers and antennas.
- By exploiting the intrinsic relationship between SCSI and the scattering environment of wireless channel, we transform the SCSI acquisition problem into a mapping construction problem between SCSI and location. To reduce the storage overhead of location-specific SCSI, the coverage area of the BS is divided into spatial grids, where the locations within each grid share the common SCSI. By collecting the noisy received signals within each grid, we formulate the mapping construction problem as a tensor decomposition problem, where the factor matrices are parameterized by the multi-path power, delay, and angle. By exploiting the Vandermonde structure of the factor matrices, the SCSI within each grid can be acquired via Vandermonde-structured tensor decomposition (VSTD) algorithm, with tensor operations significantly reducing the computational complexity.

Organization: The remainder of this paper is organized as follows. Section II describes the system model. The SA-BCE and SA-WBCE, along with the location-specific SCSI database, are detailed in Section III. In Section IV, we for-

mulate the location-specific SCSI database construction into a tensor decomposition problem and develop a VSTD-based SCSI database construction method. Simulation results are given in Section V. Finally, Section VI concludes this paper.

Notations: $\mathbf{I}_M$ is the $M \times M$ identity matrix. The imaginary unit is represented by $\bar{\jmath} = \sqrt{-1}$. $x, \mathbf{x}, \mathbf{X}$, and $\boldsymbol{\mathcal{X}}$ denote scalars, column vectors, matrices, and tensors, respectively. The superscripts $\{\cdot\}^*$, $\{\cdot\}^T$,$\{\cdot\}^H$, $\{\cdot\}^{-1}$ and $(\cdot)^\dagger$ denote the conjugate, transpose, conjugate transpose, inverse and pseudo-inverse respectively. $||\cdot||_{\mathrm{F}}$ and $||\cdot||_2$ denote the Frobenius norm and the l_2 norm, respectively. $\otimes$, $\odot$ and $\circ$ denote the Kronecker, Khatri-Rao and outer products, respectivelv. $\mathcal{CN}\left(\mu, \sigma^2\right)$ denotes a Gaussian distribution with mean μ and variance σ^2. The Kronecker delta function is represented by $\delta[\cdot]$. $\mathbb{E}\{\cdot\}$ denotes the statistic expectation. $\mathrm{diag}\{\cdot\}$ denote the diagonal operator. $\mathrm{r}(\mathbf{A})$ and $\mathrm{kr}(\mathbf{A})$ denote the rank and Kruskal-rank of $\mathbf{A}$, respectively. $[\mathbf{A}]_{:,m}$, $[\mathbf{A}]_{m:n,:}$ and $[\mathbf{A}]_{:,m:n}$ denote the m-th column of $\mathbf{A}$, the submatrix of $\mathbf{A}$ from the m-th to the n-th rows, and the submatrix of $\mathbf{A}$ from the m-th to the n-th columns, respectively. $[\cdot]_{i_1,\ldots,i_D}$ is the $(i_1,\ldots,i_D)$-th element of D-order tensor.

II. System Model

We consider a single-cell massive multiple-input multiple-output orthogonal frequency-division multiplexing (MIMO-OFDM) uplink system, where the BS is equipped with a uniform planar array (UPA) with half-wavelength antenna spacing and serves K users with an omni-directional antenna. The UPA with $M = M_{\mathrm{v}} M_{\mathrm{h}}$ antennas comprises M_{v} and M_{h} antennas in vertical and horizontal directions, respectively. OFDM modulation is employed with N_{FFT} subcarriers, and the number of subcarriers for data transmission is N_{c}, with a subcarrier spacing of Δf. The system sampling interval and OFDM symbol duration are given by $T_{\mathrm{sam}} = \frac{1}{N_{\mathrm{FFT}} \Delta f}$ and $T_{\mathrm{sym}} = \frac{1}{\Delta f}$, respectively.

A. Uplink DMRS Configuration

In the physical uplink shared channel (PUSCH), DMRS is employed to acquire CSI for subsequent coherent detection. In MU-MIMO systems, the pilot signals transmitted from different users are superimposed at the receiver. To extract individual signals from the superimposed signal, the DMRS sequence is scheduled to support multiple orthogonal ports at the transmitter. In 3GPP Release 18, Type II DMRS is specified to support a larger number of users, which divides the resource grid into multiple code division multiplexing (CDM) groups, wherein OCC are employed within each CDM group to distinguish the different orthogonal pilot ports. In particular, the maximum number of orthogonal pilot ports for Type II DMRS in 3GPP Release 18 is 24, supporting up to 24 users for uplink transmission. Fig. 1 illustrates the pilot pattern of Type II DMRS in a resource block, where the pilot pattern remains consistent across all resource blocks. Within each CDM group, frequency-domain OCC and time-domain OCC are assigned to adjacent OFDM symbols to maintain orthogonality. In this pilot configuration, the number of subcarriers occupied by each CDM group is $N = \frac{N_{\mathrm{c}}}{G}$, where G represents the number of CDM groups. The number of OFDM symbols occupied by the pilots is T_{p}.

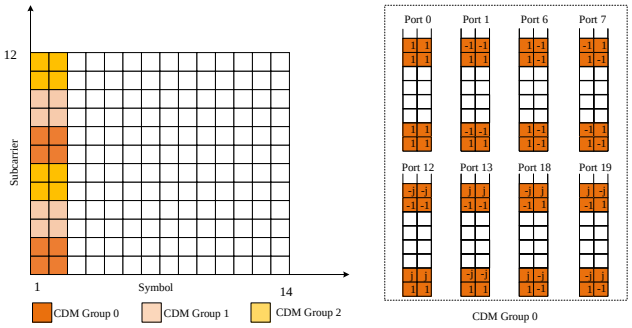

(a) DMRS mapping on resource grid (b) OCC of CDM group 0

Fig. 1: Type II DMRS pattern

B. Signal Model

Under the aforementioned pilot configuration, the number of users in each CDM group is $\frac{K}{G}$. Without loss of generality, we assume that users with index of $\{\frac{iK}{G}+1, \frac{iK}{G}+2, ..., \frac{(i+1)K}{G}\}$ are assigned to CDM group i, where $i = 0, 1, ..., G-1$. The set of pilot subcarrier indices for CDM group i is denoted as $\mathcal{P}_i = \left\{ i+1+6\left(n-1\right), i+2+6\left(n-1\right) \middle| \; n = 1, 2, \cdots, \frac{N}{2} \right\}$.

Consequently, the received signal $\mathbf{Y}_i(t) \in \mathbb{C}^{N \times M}$ of CDM group i in the t-th symbol duration at the BS can be expressed as

$$\mathbf{Y}_i(t) = \sum_{k=\frac{iK}{G}+1}^{\frac{(i+1)K}{G}} w_{t,k} \mathbf{S}_i \mathbf{C}_k \mathbf{P}_i \mathbf{H}_k(t) + \mathbf{N}(t), \tag{1}$$

where $\mathbf{H}_k(t) \in \mathbb{C}^{N_{\mathrm{c}} \times M}$ represents the frequency-space domain channel for the k-th user at the t-th symbol duration, as detailed in Section II-C. $\mathbf{P}_i \in \{0,1\}^{N \times N_{\mathrm{c}}}$ is a sampling matrix used to select the pilot subcarrier set $\mathcal{P}_i$. $\mathbf{C}_k = \mathrm{diag}\left(1, e^{\bar{\jmath} 2\pi \frac{\Delta_k}{N}} \ldots, e^{\bar{\jmath} 2\pi \frac{(N-1)\Delta_k}{N}}\right) \in \mathbb{C}^{N \times N}$ represents the frequency-domain OCC of the k-th user, where $\Delta_k \in \{0, \frac{N}{4}, \frac{N}{2}, \frac{3N}{4}\}$ represents the cyclic shift of the k-th user, employed to ensure the orthogonality of the DMRS across different users. $\mathbf{S}_i = \mathrm{diag}\{\mathbf{s}_i\} \in \mathbb{C}^{N \times N}$ represents the pilot matrix of the CDM group i, satisfying $\mathbf{S}_i \mathbf{S}_i^H = \mathbf{I}_N$ due to the unit power of the pilot symbols. $\mathbf{N}(t) \in \mathbb{C}^{N \times M}$ is the complex Gaussian noise consisting of independently and identically distributed (i.i.d.) Gaussian variables which follow the i.i.d. complex Gaussian distribution $\mathcal{CN}\left(0, \sigma\right)$. $w_{t,k} \in \{1, -1\}$ represents the time-domain OCC of the k-th user at the t-th symbol duration, which satisfies[1]

$$\frac{1}{T_p} \sum_{t=1}^{T_p} w_{t,p} w_{t,q} = \begin{cases} 1, & \text{if } (p,q \in \mathcal{U}_1) \text{ or } (p,q \in \mathcal{U}_2) \\ 0, & \text{otherwise} \end{cases}, \tag{2}$$

[1]According to the DMRS configuration in 3GPP Release 18, half of the users within a CDM group share the same time-domain OCC [9]. Without loss of generality, we assume that the users in each CDM group are divided into two sets based on whether their time-domain OCCs are identical: the first set consisting of users indexed from $\frac{iK}{G}+1$ to $\frac{(2i+1)K}{2G}$, and the second set consisting of users indexed from $\frac{(2i+1)K}{2G}+1$ to $\frac{(i+1)K}{G}$. In the main context, we consider the users in the first set without loss of generality, i.e., $u \in \left\{ \frac{iK}{G}+1, \cdots, \frac{(2i+1)K}{2G} \right\}$.

where $\mathcal{U}_1 = \{\frac{iK}{G}+1,\cdots,\frac{(2i+1)K}{2G}\}$, $\mathcal{U}_2 = \{\frac{(2i+1)K}{2G}+1,\cdots,\frac{(i+1)K}{G}\}$.

C. Channel Model

The space-frequency domain channel of k-th user at t-th symbol duration can be modeled by [28]

$$\mathbf{H}_k(t) = \sum_{l=1}^{L_{t,k}} \alpha_{l,t,k}\mathbf{b}_{N_\mathrm{c}}\left(\tau_{l,t,k}\right)\mathbf{a}(\varphi_{l,t,k},\theta_{l,t,k})^T, \tag{3}$$

where $\mathbf{a}(\varphi_{l,t,k},\theta_{l,t,k}) = \mathbf{a}_\mathrm{v}(\theta_{l,t,k})\otimes\mathbf{a}_\mathrm{h}(\varphi_{l,t,k};\theta_{l,t,k}) \in \mathbb{C}^{M\times 1}$, and $L_{t,k}$ denotes the number of multi-paths for the k-th user at the t-th symbol duration. $\alpha_{l,t,k}$, $\tau_{l,t,k}$, $\theta_{l,t,k}$, and $\varphi_{l,t,k}$ represent the complex gain, the path delay, the elevation angle of arrival (AoA), and the azimuth AoA of the l-th path for k-th user during the t-th symbol duration, respectively. $\mathbf{b}_{N_\mathrm{c}}(\tau) \in \mathbb{C}^{N_\mathrm{c}\times 1}$, $\mathbf{a}_\mathrm{v}(\theta) \in \mathbb{C}^{M_\mathrm{v}\times 1}$ and $\mathbf{a}_\mathrm{h}(\varphi;\theta) \in \mathbb{C}^{M_\mathrm{h}\times 1}$ represent the steering vectors in the delay, elevation angle and azimuth angle domains, which are defined as $\left[\mathbf{b}_{N_\mathrm{c}}(\tau)\right]_n = e^{-\bar{\jmath}2\pi n\Delta f\tau}$, $\left[\mathbf{a}_\mathrm{v}(\theta)\right]_n = e^{-\bar{\jmath}\pi n\cos\theta}$ and $\left[\mathbf{a}_\mathrm{h}(\varphi,\theta)\right]_n = e^{-\bar{\jmath}\pi n\sin\theta\cos\varphi}$, respectively.

We assume an uncorrelated fading environment, where different propagation paths are independent. Therefore, the complex gain satisfies [29]

$$\mathrm{E}\left[\alpha_{l,t,k}\alpha^*_{l',t,k}\right] = \rho_{l,t,k}\delta\left[l-l'\right], \tag{4}$$

where $\rho_{l,t,k}$ denotes the power of the l-th path for the k-th user during the t-th symbol duration. The path power $\rho_{l,t,k}$ is assumed frequency-invariant, as the frequency dependence of large-scale path loss is negligible when the system bandwidth is much smaller than the carrier frequency.

III. SCSI-Assisted Channel Estimation and Location-Specific SCSI Database

The channel estimation problem for CDM group i can be formulated as the following optimization problem, given by

$$\min_{\{\mathbf{H}_k(t)\}_{k=\frac{iK}{G}+1}^{\frac{(i+1)K}{G}}} \sum_{t=1}^{T_p}\left\|\mathbf{Y}_i(t) - \sum_{k=\frac{iK}{G}+1}^{\frac{(i+1)K}{G}} w_{t,k}\mathbf{S}_i\mathbf{C}_k\mathbf{H}_k^{\mathrm{PS}}(t)\right\|_\mathrm{F}^2, \tag{5}$$

where $\mathbf{H}_k^{\mathrm{PS}}(t) = \mathbf{P}_i\mathbf{H}_k(t) \in \mathbb{C}^{N\times M}$ represents the frequency-space domain channel of the pilot segment for the k-th user at the t-th symbol duration. In the above optimization problem, the number of channel parameters to be estimated is $\frac{KN_\mathrm{c}MT_p}{G}$, whereas the number of received signal is NMT_p, resulting in an under-determined estimation problem.

The trivial approach [10] to solving (5) consists of least-squares (LS) channel estimation, followed by time- and frequency-domain OCC decomposition, and finally, linear interpolation. However, this approach faces challenges in frequency-selective fading channels and becomes increasingly ineffective as the number of users grows. On one hand, it assumes that the channel coefficients remain unchanged over consecutive subcarriers, which does not hold under frequency-selective fading resulting from multipath propagation in complicated scattering environments. On the other hand, since the trivial approach does not incorporate inter-subcarrier correlations in OCC decoupling, its channel estimation performance deteriorates with increased pilot interference. To address these limitations, we first propose SA-BCE and SA-WBCE based on the MMSE criterion. Subsequently, we propose a location-specific SCSI database to facilitate efficient SCSI acquisition.

A. SCSI-Assisted Bayesian Channel Estimator

To address the limitations of the trivial approach, we propose the SA-BCE, which retains the first and second steps of the trivial method while introducing improvements in the subsequent stages. Specifically, the received signal $\mathbf{Y}_i(t)$ is first divided by the pilot signal $\mathbf{S}_i$ to perform LS channel estimation, as shown by

$$\hat{\mathbf{Y}}_i^{\mathrm{LS}}(t) = \mathbf{S}_i^H\mathbf{Y}_i(t) = \sum_{k=\frac{iK}{G}+1}^{\frac{(i+1)K}{G}} w_{t,k}\mathbf{C}_k\mathbf{H}_k^{\mathrm{PS}}(t) + \mathbf{S}_i^H\mathbf{N}(t), \tag{6}$$

where $\hat{\mathbf{Y}}_i^{\mathrm{LS}}(t) \in \mathbb{C}^{N\times M}$ denotes the LS channel estimation result for the pilot segment during the t-th symbol duration.

Assuming that the channel coefficients remain constant across consecutive OFDM symbols[2], the effect of the time-domain OCC in $\hat{\mathbf{Y}}_i^{\mathrm{LS}}(t)$ can be eliminated by exploiting its orthogonality property, as shown in equation (2), through

$$\hat{\mathbf{Y}}_i^{\mathrm{LS}} = \frac{1}{T_p}\sum_{t=1}^{T_p} w_{t,u}\hat{\mathbf{Y}}_i^{\mathrm{LS}}(t) = \sum_{k\in\mathcal{U}_1}\mathbf{C}_k\mathbf{H}_k^{\mathrm{PS}} + \mathbf{Z}, \tag{7}$$

where $\mathbf{H}_k^{\mathrm{PS}} = \frac{1}{T_p}\sum_{t=1}^{T_p}\mathbf{H}_k^{\mathrm{PS}}(t) \in \mathbb{C}^{N\times M}$, $\mathbf{Z} = \frac{1}{T_p}\sum_{t=1}^{T_p} w_{t,u}\mathbf{S}_i^H\mathbf{N}(t) \in \mathbb{C}^{N\times M}$.

After the time-domain OCC decoupling, rather than adopting the straightforward approach which leverages the orthogonality of frequency-domain OCC to achieve OCC decomposition, the MMSE criterion is employed to decompose the frequency-domain OCC in $\hat{\mathbf{Y}}_i^{\mathrm{LS}}$. A key prerequisite for the MMSE-based algorithms is the availability of the second-order SCSI, which can be obtained through several approaches in practical systems. For example, it can be estimated in real time using sounding reference signals (SRSs) [14] [18], or alternatively acquired from a location-specific SCSI database [27]. Therefore, it is reasonable to assume that the required second-order SCSI is available to the estimator.

With the availability of SCSI as discussed above, we proceed to present the MMSE-based estimator. Since the processing is identical across all receive antennas during the decomposition of the frequency-domain OCC, we focus on the m-th receive antenna without loss of generality. The corresponding frequency-domain received signal vector can be expressed as

$$\hat{\mathbf{y}}_i^{\mathrm{LS}} = \sum_{k=\frac{iK}{G}+1}^{\frac{(2i+1)K}{2G}}\mathbf{C}_k\mathbf{h}_k^{\mathrm{PS}} + \mathbf{z}, \tag{8}$$

[2]Considering the velocity of the user $v = 3$ km/h, the carrier frequency $f_c = 6.7$ GHz, the coherence time [28] T_c is around 20 ms, which is much longer than the OFDM symbol duration $T_{\mathrm{sym}} = 33.3$us for $\Delta f = 30$ kHz [9]. Consequently, the channel coefficients can be assumed to remain unchanged between consecutive OFDM symbols.

where $\mathbf{z} = [\mathbf{Z}]_{:,m} \in \mathbb{C}^{N\times 1}$ denotes the noise vector at the m-th antenna, $\hat{\mathbf{y}}_i^{\mathrm{LS}} = [\hat{\mathbf{Y}}_i^{\mathrm{LS}}]_{:,m} \in \mathbb{C}^{N\times 1}$ denotes the frequency-domain received signal at the m-th antenna and $\mathbf{h}_k^{\mathrm{PS}} = [\mathbf{H}_k^{\mathrm{PS}}]_{:,m} \in \mathbb{C}^{N\times 1}$ represents the frequency-domain channel of the pilot segment for the k-th user at the m-th antenna. The MMSE channel estimation of $\mathbf{h}_u^{\mathrm{PS}}$ can then be obtained according to [30]:

$$\hat{\mathbf{h}}_u^{\mathrm{PS}} = \mathbf{R}_{\mathbf{h}_u^{\mathrm{PS}}\hat{\mathbf{y}}_i^{\mathrm{LS}}}\mathbf{R}^{-1}_{\hat{\mathbf{y}}_i^{\mathrm{LS}}\hat{\mathbf{y}}_i^{\mathrm{LS}}}\hat{\mathbf{y}}_i^{\mathrm{LS}}, \tag{9}$$

where $\mathbf{R}_{\mathbf{h}_u^{\mathrm{PS}}\hat{\mathbf{y}}_i^{\mathrm{LS}}} \in \mathbb{C}^{N\times N}$ and $\mathbf{R}_{\hat{\mathbf{y}}_i^{\mathrm{LS}}\hat{\mathbf{y}}_i^{\mathrm{LS}}} \in \mathbb{C}^{N\times N}$ can be expressed as

$$\begin{aligned}
\mathbf{R}_{\mathbf{h}_u^{\mathrm{PS}}\hat{\mathbf{y}}_i^{\mathrm{LS}}} &= \mathbb{E}\left\{\mathbf{h}_u^{\mathrm{PS}}\left(\hat{\mathbf{y}}_i^{\mathrm{LS}}\right)^H\right\} = \mathbf{P}_i\mathbf{R}_u^f\mathbf{P}_i^T\mathbf{C}_u^H,\\
\mathbf{R}_{\hat{\mathbf{y}}_i^{\mathrm{LS}}\hat{\mathbf{y}}_i^{\mathrm{LS}}} &= \mathbb{E}\left\{\hat{\mathbf{y}}_i^{\mathrm{LS}}\left(\hat{\mathbf{y}}_i^{\mathrm{LS}}\right)^H\right\}\\
&= \sum_{k=\frac{iK}{G}+1}^{\frac{(2i+1)K}{2G}} \mathbf{C}_k\mathbf{P}_i\mathbf{R}_k^f\mathbf{P}_i^T\mathbf{C}_k^H + \sigma^2\mathbf{I}_N.
\end{aligned} \tag{10}$$

Here, $\mathbf{R}_k^f \in \mathbb{C}^{N_{\mathrm{c}}\times N_{\mathrm{c}}}$ denotes the frequency-domain channel correlations for the k-th user and is expressed as

$$\mathbf{R}_k^f = \sum_{l=1}^{L_{t,k}} \rho_{l,t,k}\mathbf{b}_{N_{\mathrm{c}}}(\tau_{l,t,k})\,\mathbf{b}_{N_{\mathrm{c}}}^H(\tau_{l,t,k}). \tag{11}$$

As a result, $\{\hat{\mathbf{H}}_u^{\mathrm{PS}}\}_{u=1}^K$, denoting the user-specific channel estimates based on the MMSE criterion with other-user signals treated as interference, are obtained by applying (9) to the received signals $\hat{\mathbf{y}}_i^{\mathrm{LS}}$ from all CDM groups and receive antennas, i.e,

$$\hat{\mathbf{H}}_u^{\mathrm{PS}} = \mathbf{P}_i\mathbf{R}_u^f\mathbf{P}_i^T\mathbf{C}_u^H\Big(\sum_{k=\frac{iK}{G}+1}^{\frac{(2i+1)K}{2G}} \mathbf{C}_k\mathbf{P}_i\mathbf{R}_k^f\mathbf{P}_i^T\mathbf{C}_k^H + \sigma^2\mathbf{I}_N\Big)^{-1}\hat{\mathbf{Y}}_i^{\mathrm{LS}}. \tag{12}$$

To further suppress the noise in $\hat{\mathbf{H}}_u^{\mathrm{PS}}$, we exploit the inter-antenna correlations and employ the MMSE channel estimation in the antenna domain, which gives [30]

$$(\widetilde{\mathbf{H}}_u^{\mathrm{PS}})^T = \mathbf{R}_u^s(\mathbf{R}_u^s + \sigma^2\mathbf{I}_M)^{-1}(\hat{\mathbf{H}}_u^{\mathrm{PS}})^T, \tag{13}$$

where $\mathbf{R}_u^s \in \mathbb{C}^{M\times M}$ is the antenna domain channel correlations for the u-th user, expressed as

$$\mathbf{R}_u^s = \sum_{l=1}^{L_{t,u}} \rho_{l,t,u}\mathbf{a}(\varphi_{l,t,u},\theta_{l,t,u})\mathbf{a}^H(\varphi_{l,t,u},\theta_{l,t,u}). \tag{14}$$

Finally, the full-frequency domain channel for all users, represented as $\{\hat{\mathbf{H}}_u^{\mathrm{MMSE}} \in \mathbb{C}^{N_{\mathrm{c}}\times M}\}_{u=1}^K$, is reconstructed by applying frequency-domain linear interpolation to the pilot segment channel $\{\widetilde{\mathbf{H}}_u^{\mathrm{PS}} \in \mathbb{C}^{N\times M}\}_{u=1}^K$.

B. Low-Complexity SA-BCE

The overall complexity of SA-BCE is dominated by matrix inversion with complexities of $\mathcal{O}(N^3 + M^3)$. To reduce the computational complexity of SA-BCE, we implement the SA-BCE in (9) - (14) in the beam-delay domain [31] [32] [33], thereby exploiting the limited scattering nature of wireless channels to reduce complexity. Specifically, the beam-delay domain MMSE estimator is given by

$$\begin{aligned}
\hat{\mathbf{H}}_u^{\mathrm{PS}} &= \mathbf{C}_u^H\mathbf{F}_N\mathbf{R}_u^\tau\Big(\sum_{k=\frac{iK}{G}+1}^{\frac{(2i+1)K}{2G}} \mathbf{R}_k^\tau + \sigma^2\mathbf{I}_N\Big)^{-1}\mathbf{F}_N^H\hat{\mathbf{Y}}_i^{\mathrm{LS}},\\
(\widetilde{\mathbf{H}}_u^{\mathrm{PS}})^T &= \mathbf{F}^A\mathbf{R}_u^a(\mathbf{R}_u^a + \sigma^2\mathbf{I}_M)^{-1}\left(\mathbf{F}^A\right)^H(\hat{\mathbf{H}}_u^{\mathrm{PS}})^T,
\end{aligned} \tag{15}$$

where $\mathbf{F}_N \in \mathbb{C}^{N\times N}$ denotes the discrete fourier transform (DFT) matrix, with its (i,j)-th entry defined as $[\mathbf{F}_N]_{i,j} \triangleq \frac{1}{\sqrt{N}}e^{-\bar{\jmath}2\pi\frac{ij}{N}}$, $\mathbf{F}^A = (\mathbf{F}_{M_{\mathrm{v}}} \otimes \mathbf{F}_{M_{\mathrm{h}}})$. $\mathbf{R}_u^\tau \in \mathbb{C}^{N\times N}$ and $\mathbf{R}_u^a \in \mathbb{C}^{M\times M}$ denote the delay- and beam-domain channel correlations of the u-th user, respectively, and are defined as

$$\begin{aligned}
\mathbf{R}_u^\tau &= \mathbf{F}_N^H\mathbf{C}_u\mathbf{P}_i\mathbf{R}_u^f\mathbf{P}_i^T\mathbf{C}_u^H\mathbf{F}_N = \sum_{l=1}^{L_{t,u}} \rho_{l,t,u}\overline{\mathbf{b}}(\tau_{l,t,u})\overline{\mathbf{b}}^H(\tau_{l,t,u}),\\
\mathbf{R}_u^a &= (\mathbf{F}^A)^H\mathbf{R}_u^s\mathbf{F}^A = \sum_{l=1}^{L_{t,u}} \rho_{l,t,u}\overline{\mathbf{a}}(\varphi_{l,t,u},\theta_{l,t,u})\overline{\mathbf{a}}^H(\varphi_{l,t,u},\theta_{l,t,u}),
\end{aligned} \tag{16}$$

where $\overline{\mathbf{b}}(\tau_{l,t,u}) = \mathbf{F}_N^H\mathbf{C}_u\mathbf{P}_i\mathbf{b}_{N_{\mathrm{c}}}(\tau_{l,t,u})$, $\overline{\mathbf{a}}(\varphi_{l,t,u},\theta_{l,t,u}) = \overline{\mathbf{a}}_{\mathrm{v}}(\theta_{l,t,u}) \otimes \overline{\mathbf{a}}_{\mathrm{h}}(\varphi_{l,t,u};\theta_{l,t,u})$, $\overline{\mathbf{a}}_{\mathrm{v}}(\theta_{l,t,u}) = \mathbf{F}_{M_{\mathrm{v}}}^H\mathbf{a}_{\mathrm{v}}(\theta_{l,t,u})$ and $\overline{\mathbf{a}}_{\mathrm{h}}(\varphi_{l,t,u};\theta_{l,t,u}) = \mathbf{F}_{M_{\mathrm{h}}}^H\mathbf{a}_{\mathrm{h}}(\varphi_{l,t,u};\theta_{l,t,u})$.

Since the beam-delay domain formulation is derived through a unitary transformation of the antenna-frequency domain model, the received signal models in both domains are therefore mathematically equivalent. Building on this equivalence, the corresponding MMSE estimators preserve this equivalence, as formally established in the following lemma.

Lemma 1: The beam-delay domain MMSE estimator is equivalent to its antenna-frequency domain counterpart.

Proof: Utilizing the orthogonality property of the DFT matrix $\mathbf{F}_N$ and the relation in (16), substitution of (9) and (13) directly yields the estimator in (15), thereby proving the equivalence. ■

Owing to the intrinsic sparsity of the beam–delay domain channel, the matrices $\mathbf{R}_u^\tau$ and $\mathbf{R}_u^a$ exhibit sparse structures, thereby enabling a significant reduction in the computational complexity. Specifically, we present the following proposition to characterize the asymptotic behavior of $\mathbf{R}_u^\tau$ and $\mathbf{R}_u^a$.

Proposition 1: In the infinite case, $\mathbf{R}_u^\tau$ and $\mathbf{R}_u^a$ respectively converge to diagonal matrices.

Proof: In the infinite case where both the number of antennas and subcarriers tend to infinite, the sampled steering vectors exhibit asymptotic orthogonality [34], rendering $\overline{\mathbf{b}}(\tau_{l,t,u})$ and $\overline{\mathbf{a}}(\varphi_{l,t,u},\theta_{l,t,u})$ asymptotically 1-sparse [16], i.e., containing only a single non-zero element. Consequently, according to (16), both $\mathbf{R}_u^\tau$ and $\mathbf{R}_u^a$ reduce to diagonal matrices in this case. This completes the proof. ■

Proposition 1 reveals that the beam-delay domain MMSE estimator degenerates into a element-wise operation as the number of antennas and subcarriers tends to infinity, thereby eliminating the need for matrix inversion. However, in practical systems, the number of antennas and subcarriers is finite, leading to inevitable energy leakage in the beam-delay domain. Therefore, both the beam- and delay-domain channel correlation matrices exhibit significant off-diagonal elements, which in turn substantially increases the computational complexity of the beam-delay domain MMSE estimator.

To alleviate the energy leakage problem, we incorporate the energy-concentrating property of window functions [35] [36] into the beam-delay domain MMSE estimator to develop the SA-WBCE, given by

$$\begin{aligned}\hat{\mathbf{H}}_u^{\mathrm{PS}} &= \mathbf{\Lambda}_f^{-1}\mathbf{C}_u^H\mathbf{F}_N\widetilde{\mathbf{R}}_u^{\tau}(\sum_{k=\frac{iK}{G}+1}^{\frac{(2i+1)K}{2G}}\widetilde{\mathbf{R}}_k^{\tau}+\sigma^2\mathbf{\Xi}_f)^{-1}\mathbf{F}_N^H\mathbf{\Lambda}_f\hat{\mathbf{Y}}_i^{\mathrm{LS}},\\ (\widetilde{\mathbf{H}}_u^{\mathrm{PS}})^T &= \mathbf{\Lambda}_s^{-1}\mathbf{F}^A\widetilde{\mathbf{R}}_u^a(\widetilde{\mathbf{R}}_u^a+\sigma^2\mathbf{\Xi}_s)^{-1}\left(\mathbf{F}^A\right)^H\mathbf{\Lambda}_s(\hat{\mathbf{H}}_u^{\mathrm{PS}})^T,\end{aligned} \tag{17}$$

where $\mathbf{\Xi}_f = \mathbf{F}_N^H|\mathbf{\Lambda}_f|^2\mathbf{F}_N$, $\mathbf{\Xi}_s = \left(\mathbf{F}^A\right)^H|\mathbf{\Lambda}_s|^2\mathbf{F}^A$, $\mathbf{\Lambda}_f \triangleq \mathrm{diag}\{\boldsymbol{\eta}_f\} \in \mathbb{C}^{N\times N}$ and $\mathbf{\Lambda}_s \triangleq \mathrm{diag}\{\boldsymbol{\eta}_s\} \in \mathbb{C}^{M\times M}$ denote the frequency- and antenna-domain window functions, respectively. $\widetilde{\mathbf{R}}_u^{\tau} \in \mathbb{C}^{N\times N}$ and $\widetilde{\mathbf{R}}_u^{a} \in \mathbb{C}^{M\times M}$ denote the windowed versions of the delay- and beam-domain channel correlations for the u-th user, respectively, and are given by

$$\begin{aligned}\widetilde{\mathbf{R}}_u^{\tau} &= \mathbf{F}_N^H\mathbf{\Lambda}_f\mathbf{C}_u\mathbf{P}_i\mathbf{R}_u^f\mathbf{P}_i^T\mathbf{C}_u^H\mathbf{\Lambda}_f^H\mathbf{F}_N\\ &= \sum_{l=1}^{L_{t,u}}\rho_{l,t,u}\widetilde{\mathbf{b}}(\tau_{l,t,u})\widetilde{\mathbf{b}}^H(\tau_{l,t,u}),\\ \widetilde{\mathbf{R}}_u^{a} &= (\mathbf{F}^A)^H\mathbf{\Lambda}_s\mathbf{R}_u^s\mathbf{\Lambda}_s^H\mathbf{F}^A\\ &= \sum_{l=1}^{L_{t,u}}\rho_{l,t,u}\widetilde{\mathbf{a}}(\varphi_{l,t,u},\theta_{l,t,u})\widetilde{\mathbf{a}}^H(\varphi_{l,t,u},\theta_{l,t,u}),\end{aligned} \tag{18}$$

where $\widetilde{\mathbf{b}}(\tau_{l,t,u})$ and $\widetilde{\mathbf{a}}(\varphi_{l,t,u},\theta_{l,t,u})$ represent the windowed versions of $\overline{\mathbf{b}}(\tau_{l,t,u})$ and $\overline{\mathbf{a}}(\varphi_{l,t,u},\theta_{l,t,u})$, respectively, exhibiting improved energy concentration. This implies that $\widetilde{\mathbf{R}}_u^{\tau}$ and $\widetilde{\mathbf{R}}_u^{a}$ can be approximated as band matrices $\widehat{\mathbf{R}}_u^{\tau}$ and $\widehat{\mathbf{R}}_u^{a}$, i.e.,

$$\left[\widehat{\mathbf{R}}_u^{\phi}\right]_{i,j} = \begin{cases}\left[\widetilde{\mathbf{R}}_u^{\phi}\right]_{i,j}, & \text{if } |i-j|\le B_\phi,\\ 0, & \text{otherwise,}\end{cases} \tag{19}$$

where $\phi \in \{\tau, a\}$. Due to the characteristics of the window functions, both $\mathbf{\Xi}_f$ and $\mathbf{\Xi}_s$ are band matrices with narrow band sizes. As a result, the matrix inversion in the SA-WBCE can be simplified to the inversion of band matrices, reducing the computational complexity from $\mathcal{O}(N^3+M^3)$ to $\mathcal{O}(NB_f^2+MB_s^2)$. The proposed SA-WBCE for $\mathcal{U}_1$ is summarized in Algorithm 1. For other cases, the SA-WBCE can be readily obtained by modifying the user index accordingly.

While the preceding design of the SA-BCE and SA-WBCE algorithms assumes that SCSI are readily available, the reliable SCSI acquisition under limited SRS resources remains a key challenge in practical systems. To address this issue, a promising alternative is to exploit recent advances in positioning technologies, such as integrated sensing and communication (ISAC) [37] [38], to enable database-assisted SCSI acquisition. Specifically, a location-specific SCSI database exploits the intrinsic relationship between SCSI and the wireless propagation environment, which gives rise to a consistent mapping between user location and SCSI in stationary environments. Once the SCSI at a given location is obtained, any user positioned at that location can directly utilize the corresponding SCSI without incurring additional signaling overhead. Based on this principle, we construct a location-specific SCSI database to support efficient SCSI acquisition in the proposed framework, while the detailed database construction process is presented in Sections III-C and IV.

Algorithm 1 SA-WBCE for $\mathcal{U}_1$

Input: $\{\{\tau_{l,t,u},\varphi_{l,t,u},\theta_{l,t,u},\rho_{l,t,u}\}_{l=1}^{L_{t,u}},\mathbf{C}_u,w_{t,u}\}_{u=1,\cdots,K}$, $\{\mathbf{Y}_i(t),\mathbf{S}_i,\mathbf{P}_i\}_{i=0,\cdots,G-1}$, σ^2, $\mathbf{\Xi}_f$, $\mathbf{\Xi}_s$

for $u = 1, ..., K$ **do**
  Compute $\mathbf{R}_u^f$ and $\mathbf{R}_u^s$ via (11) and (14);
  Compute $\widehat{\mathbf{R}}_u^{\tau}$ and $\widehat{\mathbf{R}}_u^{a}$ using (18) and (19);
end for
for $i = 0, ..., G-1$ **do**
  $\hat{\mathbf{Y}}_i^{\mathrm{LS}}(t) = \mathbf{S}_i^H\mathbf{Y}_i(t)$, $t = 1, ..., T_{\mathrm{p}}$;
  $\mathbf{\Gamma} = (\sum_{k=\frac{iK}{G}+1}^{\frac{(2i+1)K}{2G}}\widehat{\mathbf{R}}_k^{\tau}+\sigma^2\mathbf{\Xi}_f)^{-1}$;
  for $u = \frac{iK}{G}+1, ..., \frac{(2i+1)K}{2G}$ **do**
    % Time-domain OCC decomposition
    $\hat{\mathbf{Y}}_i^{\mathrm{LS}} = \frac{1}{T_p}\sum_{t=1}^{T_p}w_{t,u}\hat{\mathbf{Y}}_i^{\mathrm{LS}}(t)$;
    % Frequency-domain OCC decomposition
    $\hat{\mathbf{H}}_u^{\mathrm{PS}} = \mathbf{\Lambda}_f^{-1}\mathbf{C}_u^H\mathbf{F}_N\widehat{\mathbf{R}}_u^{\tau}\mathbf{\Gamma}\mathbf{\Lambda}_f\hat{\mathbf{Y}}_i^{\mathrm{LS}}$;
    % Antenna-domain MMSE
    $\mathbf{\Omega} = (\widehat{\mathbf{R}}_u^a+\sigma^2\mathbf{\Xi}_s)^{-1}\left(\mathbf{F}^A\right)^H\mathbf{\Lambda}_s$;
    $(\widetilde{\mathbf{H}}_u^{\mathrm{PS}})^T = \mathbf{\Lambda}_s^{-1}\mathbf{F}^A\widehat{\mathbf{R}}_u^a\mathbf{\Omega}(\hat{\mathbf{H}}_u^{\mathrm{PS}})^T$;
    Perform linear interpolation to obtain $\hat{\mathbf{H}}_u^{\mathrm{MMSE}}$;
  end for
end for

Output: $\{\hat{\mathbf{H}}_u^{\mathrm{MMSE}} \in \mathbb{C}^{N\mathrm{c}\times M}, u \in \mathcal{U}_1\}$.

C. Location-Specific SCSI Database

Advancements in localization systems, such as global positioning system (GPS), laser-based systems, inertial measurement units, and integrated sensing and communication (ISAC) [37], enable efficient user localization for communication systems. This progress facilitates the availability of abundant high-quality location-tagged channel data. In this context, we propose a location-specific SCSI database that establishes a mapping between user location and SCSI to support the proposed SA-BCE and SA-WBCE. To ensure the practicality of such a database, it is essential to represent the SCSI in a compact form rather than directly storing high-dimensional correlation matrices. Given that the channel correlation matrices required by SA-BCE and SA-WBCE are uniquely determined by the parameter set $\{\tau_{l,t,u},\varphi_{l,t,u},\theta_{l,t,u},\rho_{l,t,u}\}_{l=1}^{L_{t,u}}$, it is sufficient to store only this set, which significantly reduces the storage overhead while preserving all necessary information for downstream processing.

Since the BS's position is generally fixed after deployment, the SCSI depends on the user's location at t-th OFDM symbol duration (denoted as $q(t)$) and the local propagation environment. With the assumption that the local propagation environment remains quasi-static over a longer time period $2T$ relative to the signal transmission period, i.e., the quasi-static environment assumption, the SCSI depends only on the location $q(t)$. Therefore, we can establish a mapping relationship between the user's location and the SCSI, i.e.,

$$\mathcal{C}(\cdot): q(t) \to \left\{\bar{\tau}_{q(t),l},\bar{\theta}_{q(t),l},\bar{\varphi}_{q(t),l},\bar{\rho}_{q(t),l}\right\}_{l=1}^{L_{q(t)}} \quad t \in \mathbb{T}, \tag{20}$$

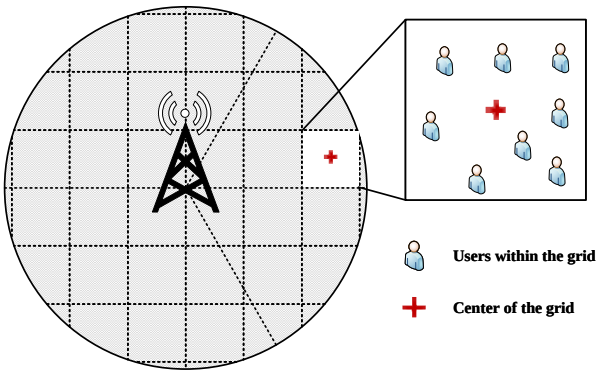

Fig. 2: Illustration of the grid-based location-specific SCSI database.

where $\mathbb{T} = \{1, \ldots, T\}$ denote the set of the OFDM symbol duration. Since the SCSI $\{\bar{\tau}_{q(t),l}, \bar{\theta}_{q(t),l}, \bar{\varphi}_{q(t),l}, \bar{\rho}_{q(t),l}\}_{l=1}^{\bar{L}_{q(t)}}$ remains unchanged over the duration of $2T$ OFDM symbols, we collect the uplink signals from the user located at $q(t)$ over T OFDM symbol durations to construct the location-specific SCSI database and use the SCSI to assist channel estimation over the subsequent T OFDM symbol durations.

However, directly mapping all possible user locations within the physical region to the SCSI incurs significant storage overhead. To address this issue, we divide the coverage area of the BS into multiple grids, where users within the same grid share a common SCSI. The rationale behind grid partitioning is the spatial consistency of wireless channels which refers to the fact that neighboring spatial positions tend to share similar clusters, leading to spatial correlation in SCSI [39]. The correlation of SCSI at two spatial positions depends on both the distance between them and the correlation distance of the environments. When the distance between the two positions exceeds the correlation distance, the corresponding SCSI of the two positions become statistically independent, and vice versa can be considered identical. Thus, as long as the grid size is much smaller than the correlation distance, the SCSI at different positions within the same grid can be approximated as identical.

In the following, we provide a detailed description of the grid-based SCSI database as shown in Fig. 2. Assume that the coverage area of the BS is divided into U grids, each with a size of $d \times d\,\mathrm{m}^2$, where d is much smaller than the correlation distance. Define a mapping $\mathcal{G}(\cdot)$ from the user's location at t-th OFDM symbol duration $q(t)$ to a grid g as

$$\mathcal{L}(\cdot) : g = \mathcal{L}(q(t)) \quad t \in \mathbb{T}, g \in \mathbb{G}, \tag{21}$$

where $\mathbb{G} = \{1, \ldots, U\}$ denote the set of the grid. Based on grid partitioning, we can replace the location-based SCSI $\{\bar{\tau}_{q(t),l}, \bar{\theta}_{q(t),l}, \bar{\varphi}_{q(t),l}, \bar{\rho}_{q(t),l}\}_{l=1}^{\bar{L}_{q(t)}}$ with the grid-based one $\{\bar{\tau}_{g,l}, \bar{\theta}_{g,l}, \bar{\varphi}_{g,l}, \bar{\rho}_{g,l}\}_{l=1}^{\bar{L}}$, where $\bar{L}$ denotes the number of effective paths of the channel. The corresponding grid-based SCSI database can be represented as

$$\mathcal{C}(\cdot) : g \to \{\bar{\tau}_{g,l}, \bar{\theta}_{g,l}, \bar{\varphi}_{g,l}, \bar{\rho}_{g,l}\}_{l=1}^{\bar{L}}. \tag{22}$$

To obtain the SCSI of user k for the DMRS channel estimation, the position $q_k(t)$ of user k at the t-th OFDM symbol is mapped to the grid g_k using the function $g_k = \mathcal{L}(q_k(t))$ in (21). Subsequently, the SCSI for grid g_k, denoted as $\{\tau_{g_k,l}, \varphi_{g_k,l}, \theta_{g_k,l}, \rho_{g_k,l}\}_{l=1}^{\bar{L}}$, is obtained by applying $\mathcal{C}(g_k)$ as given in (22). It is worth noting that, in practical systems, the processes of localization and database lookup introduces a non-negligible latency, typically on the order of milliseconds [40] [41]. For users with relatively low mobility, such millisecond-level latency does not cause significant position variation and therefore has minimal impact on the effectiveness of the location-specific SCSI database. In contrast, in high-mobility scenarios, this latency may result in noticeable position errors, potentially causing the user to be mapped to an incorrect spatial grid and consequently retrieving mismatched SCSI. To address this issue, position prediction techniques [42] [43] are required to compensate for the latency-induced errors and enhance SCSI accuracy under high mobility scenarios.

Given the obtained SCSI $\{\tau_{g_k,l}, \varphi_{g_k,l}, \theta_{g_k,l}, \rho_{g_k,l}\}_{l=1}^{\bar{L}}$, the frequency-domain channel correlation matrix $\tilde{\mathbf{R}}_k^f$ and antenna-domain channel correlation matrix $\tilde{\mathbf{R}}_k^s$ can be computed using (11) and (14). Based on $\tilde{\mathbf{R}}_k^f$ and $\tilde{\mathbf{R}}_k^s$ for all users, the channel can be estimated using the SA-BCE and SA-WBCE as detailed in Section III-A and Section III-B, respectively.

IV. VSTD-Based SCSI Database Construction

In this section, we first analyze the received signals for the location-specific SCSI database construction. Building on this foundation, we reformulate the location-specific SCSI database construction as a tensor decomposition problem, where the multilinear structure of wireless channels [44], [45] enables a significant reduction in computational complexity.

A. Received Signals for SCSI Database Construction

The grid-based SCSI database, as shown in Fig. 2, is constructed by utilizing the received signals from all users within the grid. For simplicity, we define $\mathbb{Q}_g = \{(q,t) \mid g = \mathcal{L}(q), t \in \mathbb{T}\}$ as the set of locations corresponding to grid g and their corresponding OFDM symbol duration indices. For simplicity, we define $v = (q,t) \in \mathbb{Q}_g$, as the spatial sampling point for grid g (the user at location q during the t-th OFDM symbol duration). Based on (22), the channel of the sampling point v located within grid g can be represented as

$$\mathbf{H}_v = \sum_{l=1}^{\bar{L}} \alpha_{l,v} \mathbf{b}_{N_\mathrm{d}}(\bar{\tau}_{g,l})\, \mathbf{a}(\bar{\varphi}_{g,l}, \bar{\theta}_{g,l})^T + \Delta_{\mathbf{H}_v}, v \in \mathbb{Q}_g, \tag{23}$$

where $\mathbf{H}_v \in \mathbb{C}^{N_\mathrm{d} \times M}$, and N_d denotes the number of subcarriers used to obtain the SCSI. $\alpha_{l,v}$ is the l-th effective complex coefficient, which satisfies $\mathrm{E}\left[\alpha_{l,v}\alpha_{l,v}^*\right] = \bar{\rho}_{g,l}$. $\Delta_{\mathbf{H}_v}$ represents the error in channel representation and can also indicate the accuracy of the SCSI. Over the T OFDM symbol durations, the received signals $\mathbf{Y}_v \in \mathbb{C}^{N_\mathrm{d} \times M}$, $v \in \mathbb{Q}_g$, are collected as measurement data including sounding reference signals, synchronization signals, etc., from all users within grid g. Subsequently, $\mathbf{Y}_v$, for $v \in \mathbb{Q}_g$, is used to construct the SCSI database for grid g, given by

$$\mathbf{Y}_v = \mathbf{S}_v \mathbf{H}_v + \tilde{\mathbf{N}}_v, \tag{24}$$

where $\mathbf{S}_v \in \mathbb{C}^{N_\mathrm{d}\times N_\mathrm{d}}$ denotes the pilot sequence of the sampling point v, $\tilde{\mathbf{N}}_v \in \mathbb{C}^{N_\mathrm{d}\times M}$ represents the complex Gaussian noise matrix, where each element follows the i.i.d. complex Gaussian distribution, incorporating the channel representation error induced by $\Delta_{\mathbf{H}_v}$.

To facilitate implementation, we equivalently represent $\mathbf{Y}_v$ in vector form as follows:

$$\mathbf{y}_v = \sum_{l=1}^{\bar{L}} \alpha_{l,v} \left(\mathbf{S}_v \mathbf{b}_{N_\mathrm{d}}\left(\bar{\tau}_{g,l}\right)\right) \otimes \mathbf{a}(\bar{\varphi}_{g,l}, \bar{\theta}_{g,l}) + \tilde{\mathbf{n}}_v. \tag{25}$$

Assume that there are W spatial sampling points $\{v_1, v_2, \ldots, v_W\}$ within each grid, we can use the received signals from these spatial sampling points $\{\mathbf{y}_{v_1}, \mathbf{y}_{v_2}, \ldots, \mathbf{y}_{v_w}, \ldots, \mathbf{y}_{v_W}, v_w \in \mathbb{Q}_g\}_{w=1}^{W}$ to obtain the SCSI for grid g. To eliminate the effects of pilot, we first perform LS channel estimation on the received signal $\mathbf{y}_{v_w}$, as follows:

$$\mathbf{h}_{v_w}^{\mathrm{LS}} = (\mathbf{S}_{v_w}^H \otimes \mathbf{I}_M)\mathbf{y}_{v_w}. \tag{26}$$

Let $\mathbf{H}_g \in^{N_\mathrm{d}M\times W}$ be the concatenation of the channels from all sampling points, given by

$$\mathbf{H}_g = \left[\mathbf{h}_{v_1}^{\mathrm{LS}}, \mathbf{h}_{v_2}^{\mathrm{LS}}, \ldots, \mathbf{h}_{v_w}^{\mathrm{LS}}, \ldots, \mathbf{h}_{v_W}^{\mathrm{LS}}\right], v_w \in \mathbb{Q}_g. \tag{27}$$

Since we assume that the SCSI remains consistent for each sampling point within each grid, $\mathbf{H}_g$ can be represented as

$$\mathbf{H}_g = \sum_{l=1}^{\bar{L}} \left(\mathbf{b}_{N_\mathrm{d}}\left(\bar{\tau}_{g,l}\right) \otimes \mathbf{a}(\bar{\varphi}_{g,l}, \bar{\theta}_{g,l})\right) \mathbf{p}_{g,l}^T + \mathbf{N}_g, \tag{28}$$

where $\mathbf{p}_{g,l} = [\alpha_{l,v_1}, \alpha_{l,v_2}, \ldots, \alpha_{l,v_W}]^T$ denotes the channel gains of the l-th path at all sampling points within grid g. Since α_{l,v_w} satisfies the condition $\mathbb{E}[\alpha_{l,v_w}\alpha_{l,v_w}^*] = \bar{\rho}_{l,g}, w = 1, 2, \ldots, W$, we can approximate $\bar{\rho}_{l,g}$ using α_{l,v_w} as follows:

$$\bar{\rho}_{l,g} = \frac{1}{W}\sum_{w=1}^{W} |\alpha_{l,v_w}|^2. \tag{29}$$

Since the received signals $\mathbf{y}_v$ exhibit a nonlinear relationship with the underlying SCSI parameters, traditional methods for obtaining SCSI parameters typically require iterative procedures [19], resulting in high computational complexity. To tackle this challenge and estimate the parameters efficiently, we establish a tensor decomposition framework for location-specific SCSI database construction in the following subsection.

B. Problem Formulation

We aim to extract $\bar{\tau}_{g,l}$, $\bar{\theta}_{g,l}$, $\bar{\varphi}_{g,l}$, and $\bar{\rho}_{g,l}$ from the data $\mathbf{H}_g$ to construct the SCSI database. Note that the construction of the SCSI database for each grid is independent and follows the same procedure. Without loss of generality, we present the problem formulation for the g-th grid below. Using the expression of $\mathbf{H}_g$ in (28), we first derive a fourth-order tensor $\boldsymbol{\mathcal{H}}^g \in \mathbb{C}^{N_\mathrm{d}\times M_\mathrm{v}\times M_\mathrm{h}\times W}$, with its $(n, m_\mathrm{v}, m_\mathrm{v}, w)$-th entry given by $[\mathbf{H}_g]_{nM+m_\mathrm{v}M_\mathrm{h}+m_\mathrm{h},w}$. By comparing (28) to the definition of tensor canonical polyadic decomposition (CPD) [46], it can be readily observed that $\boldsymbol{\mathcal{H}}_g$ can be represented in a CPD format, i.e.,

$$\begin{aligned}\boldsymbol{\mathcal{H}}_g &= [\![\mathbf{B}^{(1)}, \mathbf{B}^{(2)}, \mathbf{B}^{(3)}, \mathbf{B}^{(4)}]\!] + \boldsymbol{\mathcal{N}}_g \\ &= \sum_{l=1}^{\bar{L}} \mathbf{b}_{N_\mathrm{d}}\left(\bar{\tau}_{g,l}\right) \circ \mathbf{a}_\mathrm{v}(\bar{\theta}_{g,l}) \circ \mathbf{a}_\mathrm{h}(\bar{\varphi}_{g,l}, \bar{\theta}_{g,l}) \circ \mathbf{p}_{g,l} + \boldsymbol{\mathcal{N}}_g,\end{aligned} \tag{30}$$

where $\boldsymbol{\mathcal{N}}_g$ is the tensor form of noise and representation error. $\mathbf{B}^{(1)}, \mathbf{B}^{(2)}, \mathbf{B}^{(3)}$ and $\mathbf{B}^{(4)}$ are factor matrices represented by

$$\begin{aligned}\mathbf{B}^{(1)} &= \left[\mathbf{b}_{N_\mathrm{d}}\left(\bar{\tau}_{g,1}\right), \ldots, \mathbf{b}_{N_\mathrm{d}}\left(\bar{\tau}_{g,\bar{L}}\right)\right] \in \mathbb{C}^{N_\mathrm{d}\times\bar{L}}, \\ \mathbf{B}^{(2)} &= \left[\mathbf{a}_\mathrm{v}(\bar{\theta}_{g,1}), \ldots, \mathbf{a}_\mathrm{v}(\bar{\theta}_{g,\bar{L}})\right] \in \mathbb{C}^{M_\mathrm{v}\times\bar{L}}, \\ \mathbf{B}^{(3)} &= \left[\mathbf{a}_\mathrm{h}(\bar{\varphi}_{g,1}, \bar{\theta}_{g,1}), \ldots, \mathbf{a}_\mathrm{h}(\bar{\varphi}_{g,\bar{L}}, \bar{\theta}_{g,\bar{L}})\right] \in \mathbb{C}^{M_\mathrm{h}\times\bar{L}}, \\ \mathbf{B}^{(4)} &= \left[\mathbf{p}_{g,1}, \ldots, \mathbf{p}_{g,\bar{L}}\right] \in \mathbb{C}^{W\times\bar{L}}.\end{aligned} \tag{31}$$

We aim to estimate the SCSI $\{\bar{\tau}_{g,l}, \bar{\theta}_{g,l}, \bar{\varphi}_{g,l}, \bar{\rho}_{g,l}\}_{l=1}^{\bar{L}}$ from the observation tensor $\boldsymbol{\mathcal{H}}_g$, by utilizing the structured CPD format as described in (30)-(31). The SCSI estimation problem can be formulated as the following optimization problem:

$$\min_{\{\bar{\tau}_{g,l}, \bar{\theta}_{g,l}, \bar{\varphi}_{g,l}, \bar{\rho}_{g,l}\}_{l=1}^{\bar{L}}} \left\| \boldsymbol{\mathcal{H}}_g - [\![\mathbf{B}^{(1)}, \mathbf{B}^{(2)}, \mathbf{B}^{(3)}, \mathbf{B}^{(4)}]\!] \right\|_F^2. \tag{32}$$

The above problem essentially corresponds to a CPD problem, which can be addressed using existing tensor decomposition algorithms. Intuitively, these algorithms approximates the high-dimensional tensor by a set of low-dimensional factor matrices, allowing for processing in one domain while treating the other domains as batches, thereby reducing computational complexity. This decomposition not only separates the latent components across different domains but also significantly lowers the computational burden, as the factor matrices have substantially lower dimensionality compared to the original tensor.

One of the most widely used tensor decomposition algorithms is the alternating least squares (ALS) [47] method, which iteratively estimates one factor matrix while keeping the others fixed, updating them alternately. Given the estimated factor matrices $\{\mathbf{B}^{(1)}, \mathbf{B}^{(2)}, \mathbf{B}^{(3)}, \mathbf{B}^{(4)}\}$, the SCSI can be derived by leveraging the underlying manifold structure of the factor matrices. However, the ALS algorithm guarantees the uniqueness of the estimated factor matrices only when the tensor is of low rank. In contrast, the scenario considered in this paper involves a channel with several hundred sub-paths, resulting in a high-rank CPD problem for which the uniqueness condition is no longer satisfied. Since uniqueness is critical for reliable CPD-based decomposition, we first analyze the uniqueness conditions associated with the CPD formulation in equation (32). This analysis then serves as the foundation for enhancing the subsequent SCSI estimation algorithm.

C. Extraction of SCSI

The uniqueness condition of the CPD problem is fundamental to the accurate estimation of SCSI, ensuring that the decomposed factor matrices incorporate the accurate information of channel statistical parameters. A well-known sufficient

condition for the uniqueness of CPD problem (32) is as follows [48]:

Lemma 1: Considering the fourth-order tensor $\boldsymbol{\mathcal{H}}_g$ defined in (30), if the condition $\sum_{i=1}^{4} \mathrm{kr}(\mathbf{B}^{(i)}) \geq 2\bar{L}+3$ is satisfied, then the CPD of $\boldsymbol{\mathcal{H}}_g$ is guaranteed to be unique. In the general case, the uniqueness condition simplifies to

$$\min\left(N_{\mathrm{d}}, \bar{L}\right) + \min\left(M_{\mathrm{v}}, \bar{L}\right) + \min\left(M_{\mathrm{h}}, \bar{L}\right) + \min\left(W, \bar{L}\right) \geq 2\bar{L}+3 \tag{33}$$

In our system, since M_v, M_h, and W are much smaller than $\bar{L}$, the condition $\mathrm{kr}\left(\mathbf{B}^{(2)}\right) + \mathrm{kr}\left(\mathbf{B}^{(3)}\right) + \mathrm{kr}\left(\mathbf{B}^{(4)}\right) < \bar{L}$ holds. Therefore, the Kruskal condition cannot be satisfied.

To address this issue, the structural properties within the tensor must be exploited to relax the uniqueness condition. Note that the factor matrices $\mathbf{B}^{(1)}$, $\mathbf{B}^{(2)}$, and $\mathbf{B}^{(3)}$ are all Vandermonde matrices where the generators are $\{z_{1,l} = e^{-\bar{\jmath}2\pi\Delta f \bar{\tau}_{g,l}}\}_{l=1}^{\bar{L}}, \{z_{2,l} = e^{-\bar{\jmath}\pi\cos\bar{\theta}_{g,l}}\}_{l=1}^{\bar{L}}$ and $\{z_{3,l} = e^{-\bar{\jmath}\pi\sin\bar{\theta}_{g,l}\cos\bar{\varphi}_{g,l}}\}_{l=1}^{\bar{L}}$ respectively. Utilizing this structural information, the following relaxed uniqueness condition can be derived [10], [49].

Lemma 2: Considering the fourth-order tensor $\boldsymbol{\mathcal{H}}_g$ defined in (30), where $\mathbf{B}^{(1)}, \mathbf{B}^{(2)}, \mathbf{B}^{(3)}$ are Vandermonde matrix with generators $\{z_{1,l}\}_{l=1}^{\bar{L}}, \{z_{2,l}\}_{l=2}^{\bar{L}}, \{z_{3,l}\}_{l=1}^{\bar{L}}$. Select the smoothing parameters $(K_s, L_s), s = 1,2,3$ subject to $K_1 + L_1 = N_{\mathrm{d}} + 1$, $K_2 + L_2 = M_{\mathrm{v}} + 1$, and $K_3 + L_3 = M_{\mathrm{h}} + 1$ for spatial smoothing. If

$$\begin{aligned} &z_{1,i} \neq z_{1,j}, \forall i \neq j, \\ &\mathrm{r}\left(\mathbf{B}^{(K_1-1,1)} \odot \mathbf{B}^{(K_2,2)} \odot \mathbf{B}^{(K_3,3)}\right) = \bar{L}, \\ &\mathrm{r}\left(\mathbf{B}^{(L_1,1)} \odot \mathbf{B}^{(L_2,2)} \odot \mathbf{B}^{(L_3,3)} \odot \mathbf{B}^{(4)}\right) = \bar{L}, \end{aligned} \tag{34}$$

then the CPD of $\boldsymbol{\mathcal{H}}_g$ is unique. Specifically, $\mathbf{B}^{(K_1-1,1)} \triangleq [\mathbf{B}^{(1)}]_{1:K_1-1,:}$ denotes the first K_1-1 rows of $\mathbf{B}^{(1)}$. In general, condition (34) simplifies to

$$\min\left(\left(K_1-1\right)K_2K_3, L_1L_2L_3I_4\right) \geq \bar{L}. \tag{35}$$

The relaxed uniqueness condition (35) can be guaranteed by appropriately choosing parameters $(K_s, L_s), s = 1,2,3$.

Based on Lemma 2, the high-rank CPD problem in our work can be solved by exploiting the Vandermonde structure of the factor matrices. Specifically, we leverage the method in [10] and [49] to estimate the SCSI of grid g using $\boldsymbol{\mathcal{H}}_g$. We define the smoothing parameters $(K_s, L_s), s = 1,2,3$, which satisfy the conditions outlined in Lemma 2. Consider the matricization $\mathbf{X}^{[3]}$ of the tensor $\boldsymbol{\mathcal{H}}_g$ [49] as follows:

$$\begin{aligned} &\mathbf{X}^{[3]} \\ &\triangleq \begin{bmatrix} [\boldsymbol{\mathcal{H}}_g]_{1,1,1,1} & [\boldsymbol{\mathcal{H}}_g]_{1,1,1,1} & \cdots & [\boldsymbol{\mathcal{H}}_g]_{1,1,1,W} \\ [\boldsymbol{\mathcal{H}}_g]_{1,1,2,1} & [\boldsymbol{\mathcal{H}}_g]_{1,1,2,1} & \cdots & [\boldsymbol{\mathcal{H}}_g]_{1,1,2,W} \\ \vdots & \vdots & \ddots & \vdots \\ [\boldsymbol{\mathcal{H}}_g]_{N_{\mathrm{d}},M_{\mathrm{v}},M_{\mathrm{h}},1} & [\boldsymbol{\mathcal{H}}_g]_{N_{\mathrm{d}},M_{\mathrm{v}},M_{\mathrm{h}},2} & \cdots & [\boldsymbol{\mathcal{H}}_g]_{N_{\mathrm{d}},M_{\mathrm{v}},M_{\mathrm{h}},W} \end{bmatrix} \\ &= \left(\mathbf{B}^{(1)} \odot \mathbf{B}^{(2)} \odot \mathbf{B}^{(3)}\right)\mathbf{P}_g^T + \mathbf{N}^{[3]}, \end{aligned} \tag{36}$$

where $\mathbf{N}^{[3]} \in \mathbb{C}^{N_{\mathrm{d}}M_{\mathrm{v}}M_{\mathrm{h}} \times W}$ is the corresponding noise matrix. Since $\mathbf{B}^{(1)}, \mathbf{B}^{(2)}$, and $\mathbf{B}^{(3)}$ exhibit a Vandermonde structure, the dimension of $\mathbf{X}^{[3]}$ can be expanded by exploiting the spatial smoothing technique. We perform spatial smoothing on $\mathbf{X}^{[3]}$, yielding

$$\begin{aligned} \mathbf{X}_{\mathcal{S}} \triangleq &\left[\begin{array}{cccccc} \mathbf{J}_{1,1,1}\mathbf{X}^{[3]} & \cdots & \mathbf{J}_{1,1,L_3}\mathbf{X}^{[3]} & \cdots & \mathbf{J}_{1,2,1}\mathbf{X}^{[3]} \\ & \cdots & \mathbf{J}_{1,2,L_3}\mathbf{X}^{[3]} & \cdots & \mathbf{J}_{1,L_2,L_3}\mathbf{X}^{[3]} \\ & & \cdots \mathbf{J}_{L_1,1,1}\mathbf{X}^{[3]} & \cdots & \mathbf{J}_{L_1,L_2,L_3}\mathbf{X}^{[3]} \end{array}\right] \\ &= \left(\mathbf{B}^{(K_1,1)} \odot \mathbf{B}^{(K_2,2)} \odot \mathbf{B}^{(K_3,3)}\right) \\ &\cdot \left(\mathbf{B}^{(L_1,1)} \odot \mathbf{B}^{(L_2,2)} \odot \mathbf{B}^{(L_3,3)} \odot \mathbf{B}^{(4)}\right)^T + \mathbf{N}_{\mathcal{S}}, \end{aligned} \tag{37}$$

where $\mathbf{N}_{\mathcal{S}} \in \mathbb{C}^{K_1K_2K_3 \times L_1L_2L_3W}$ is the corresponding noise matrix; $\mathbf{J}_{l_1,l_2,l_3}$ is the selection matrix [50], given by

$$\begin{aligned} \mathbf{J}_{l_1,l_2,l_3} \triangleq &\left[\begin{array}{ccc} \mathbf{0}_{K_1\times(l_1-1)} & \mathbf{I}_{K_1} & \mathbf{0}_{K_1\times(L_1-l_1)} \end{array}\right] \otimes \\ &\left[\begin{array}{ccc} \mathbf{0}_{K_2\times(l_2-1)} & \mathbf{I}_{K_2} & \mathbf{0}_{K_2\times(L_2-l_2)} \end{array}\right] \otimes \\ &\left[\begin{array}{ccc} \mathbf{0}_{K_3\times(l_3-1)} & \mathbf{I}_{K_3} & \mathbf{0}_{K_3\times(L_3-l_3)} \end{array}\right]. \end{aligned} \tag{38}$$

Subsequently, the truncated singular value decomposition is performed on $\mathbf{X}_{\mathcal{S}}$, i.e.,

$$\mathrm{SVD}\left(\mathbf{X}_{\mathcal{S}}\right) = \mathbf{U}\boldsymbol{\Sigma}\mathbf{V}^{\mathrm{H}}, \tag{39}$$

where $\mathbf{U} \in \mathbb{C}^{K_1K_2K_3 \times \bar{L}}, \boldsymbol{\Sigma} \in \mathbb{C}^{\bar{L}\times\bar{L}}$ and $\mathbf{V} \in \mathbb{C}^{L_1L_2L_3W\times\bar{L}}$. Using the minimum description length (MDL) criterion [51], $\bar{L}$ can be estimated.

Omitting the noise and based on (34), there exists a non-singular matrix $\mathbf{M} \in \mathbb{C}^{\bar{L}\times\bar{L}}$ such that

$$\begin{aligned} \mathbf{U}\mathbf{M} &= \mathbf{B}^{(K_1,1)} \odot \mathbf{B}^{(K_2,2)} \odot \mathbf{B}^{(K_3,3)}, \\ \mathbf{V}^*\Sigma\mathbf{N} &= \mathbf{B}^{(L_1,1)} \odot \mathbf{B}^{(L_2,2)} \odot \mathbf{B}^{(L_3,3)} \odot \mathbf{B}^{(4)}, \mathbf{N} = \mathbf{M}^{-T}. \end{aligned} \tag{40}$$

The above equation implies that

$$\begin{aligned} \mathbf{U}_1\mathbf{M} &= \underline{\mathbf{B}}^{(K_1,1)} \odot \mathbf{B}^{(K_2,2)} \odot \mathbf{B}^{(K_3,3)}, \\ \mathbf{U}_2\mathbf{M} &= \overline{\mathbf{B}}^{(K_1,1)} \odot \mathbf{B}^{(K_2,2)} \odot \mathbf{B}^{(K_3,3)}, \end{aligned} \tag{41}$$

where $\underline{\mathbf{B}}^{(K_1,1)}$ and $\overline{\mathbf{B}}^{(K_1,1)}$ are obtained by deleting the bottom and top row of $\mathbf{B}^{(K_1,1)}$ respectively, i.e., $\underline{\mathbf{B}}^{(K_1,1)} = [\mathbf{B}^{(K_1,1)}]_{1:K_1-1,:}$, $\overline{\mathbf{B}}^{(K_1,1)} = [\mathbf{B}^{(K_1,1)}]_{2:K_1,:}$. The expressions for $\mathbf{U}_1$ and $\mathbf{U}_2$ are

$$\begin{aligned} \mathbf{U}_1 &= [\mathbf{U}]_{1:(K_1-1)K_2K_3,:}, \\ \mathbf{U}_2 &= [\mathbf{U}]_{1+K_2K_3:K_1K_2K_3,:}. \end{aligned} \tag{42}$$

Due to the Vandermonde structure of $\mathbf{B}^{(1)}$, we have

$$\begin{aligned} &\left(\underline{\mathbf{B}}^{(K_1,1)} \odot \mathbf{B}^{(K_2,2)} \odot \mathbf{B}^{(K_3,3)}\right)\mathbf{Z}_1 \\ &\qquad = \overline{\mathbf{B}}^{(K_1,1)} \odot \mathbf{B}^{(K_2,2)} \odot \mathbf{B}^{(K_3,3)}, \end{aligned} \tag{43}$$

where $\mathbf{Z}_1 = \mathrm{diag}\left(\left[z_{1,1}, \ldots, z_{1,\bar{L}}\right]\right)$.

By merging (41)-(43), the following equation is obtained:

$$\mathbf{U}_1\mathbf{M}\mathbf{Z}_1 = \mathbf{U}_2\mathbf{M}. \tag{44}$$

From (44), we have $\mathbf{U}_2 = \mathbf{U}_1\widehat{\mathbf{Z}}_1$, where $\widehat{\mathbf{Z}}_1 = \mathbf{M}\mathbf{Z}_1\mathbf{M}^{-1}$. Since $\underline{\mathbf{B}}^{(K_1,1)} \odot \mathbf{B}^{(K_2,2)} \odot \mathbf{B}^{(K_3,3)}$ has full column rank, it follows that $\mathbf{U}_1$ and $\mathbf{U}_2$ also have full column rank. Therefore, we obtain $\widehat{\mathbf{Z}}_1 = \mathbf{U}_1^{\dagger}\mathbf{U}_2$. From the eigenvalue decomposition

(EVD), $\mathbf{U}_1^{\dagger}\mathbf{U}_2 = \mathbf{M}\mathbf{Z}_1\mathbf{M}^{-1}$, the Vandermonde generators set $\{z_{1,l}\}_{l=1}^{\bar{L}}$ of $\mathbf{B}^{(1)}$ is derived, i.e.,

$$\{z_{1,l}\}_{l=1}^{\bar{L}} = \mathrm{diag}(\mathbf{Z}_1), z_{1,l} = \frac{z_{1,l}}{|z_{1,l}|}, l = 1, \ldots, \bar{L}. \tag{45}$$

Then, we can reconstruct $\mathbf{B}^{(1)}$ with $\{z_{1,l}\}_{l=1}^{\bar{L}}$ based on (31). The next step is to find $\mathbf{B}^{(2)}$. Note that

$$\left(\frac{(\mathbf{b}_l^{(K_1,1)})^H}{\mathbf{b}_l^{(K_1,1)H}\mathbf{b}_l^{(K_1,1)}} \otimes \mathbf{I}_{K_2K_3}\right)\left(\mathbf{b}_l^{(K_1,1)} \otimes \mathbf{b}_l^{(K_2,2)} \otimes \mathbf{b}_l^{(K_3,3)}\right) = \mathbf{b}_l^{(K_2,2)} \otimes \mathbf{b}_l^{(K_3,3)}, \tag{46}$$

where $\mathbf{b}_l^{(K_s,s)}$ is the l-th column of $\mathbf{B}^{(K_s,s)}(s = 1, 2, 3)$. Thus, by leveraging (40), $\mathbf{b}_l^{(K_2,2)} \otimes \mathbf{b}_l^{(K_3,3)}$ is obtained as

$$\mathbf{b}_l^{(K_2,2)} \otimes \mathbf{b}_l^{(K_3,3)} = \left(\frac{\left(\mathbf{b}_l^{(K_1,1)}\right)^{\mathrm{H}}}{\left(\mathbf{b}_l^{(K_1,1)}\right)^{\mathrm{H}}\mathbf{b}_l^{(K_1,1)}} \otimes \mathbf{I}_{K_2K_3}\right)\mathbf{U}\mathbf{m}_l. \tag{47}$$

Then, the second Vandermonde generators set $\{z_{2,l}\}_{l=1}^{\bar{L}}$ of $\mathbf{B}^{(2)}$ is determined. Since $\left(\underline{\mathbf{B}}^{(K_2,2)} \odot \mathbf{B}^{(K_3,3)}\right)\mathbf{Z}_2 = \overline{\mathbf{B}}^{(K_2,2)} \odot \mathbf{B}^{(K_3,3)}$, where $\mathbf{Z}_2 = \mathrm{diag}\left(\left[z_{2,1}, \ldots, z_{2,\bar{L}}\right]\right)$, we have

$$\begin{aligned} z_{2,l} = &\left(\mathbf{b}_l^{(K_2,2)} \otimes \mathbf{b}_l^{(K_3,3)}\right)^{\dagger}_{(1:(K_2-1)K_3,1)} \\ &\cdot \left(\mathbf{b}_l^{(K_2,2)} \otimes \mathbf{b}_l^{(K_3,3)}\right)_{(K_3+1:K_2K_3,1)}. \end{aligned} \tag{48}$$

Similarly, we reconstruct $\mathbf{B}^{(2)}$ with $\{z_{2,l}\}_{l=1}^{\bar{L}}$. So far, we have obtained $\left\{\mathbf{B}^{(1)}, \mathbf{B}^{(2)}\right\}$. l-th vector of $\mathbf{B}^{(3)}$ can be derived in the similar way, i.e.,

$$\begin{aligned} \mathbf{b}_l^{(K_3,3)} = &\left(\frac{\left(\mathbf{b}_l^{(K_2,2)}\right)^{\mathrm{H}}}{\left(\mathbf{b}_l^{(K_2,2)}\right)^{\mathrm{H}}\mathbf{b}_l^{(K_2,2)}} \otimes \mathbf{I}_{K_3}\right) \\ &\cdot \left(\frac{\left(\mathbf{b}_l^{(K_1,1)}\right)^{\mathrm{H}}}{\left(\mathbf{b}_l^{(K_1,1)}\right)^{\mathrm{H}}\mathbf{b}_l^{(K_1,1)}} \otimes \mathbf{I}_{K_2K_3}\right)\mathbf{U}\mathbf{m}_l. \end{aligned} \tag{49}$$

Considering the Vandermonde structure of $\mathbf{B}^{(K_3,3)}$, the generators of $\mathbf{B}^{(3)}$ can be expressed as $z_{3,l} = \left(\underline{\mathbf{b}_l}^{(K_3,3)}\right)^{\dagger}\overline{\mathbf{b}}_l^{(K_3,3)}$. According to (40), l-th vector of $\mathbf{B}^{(4)}$ can be derived as

$$\begin{aligned} \mathbf{b}_l^{(4)} = &\frac{\left(\mathbf{b}_l^{(L_1,1)}\right)^{\mathrm{H}}}{\left(\mathbf{b}_l^{(L_1,1)}\right)^{\mathrm{H}}\mathbf{b}_l^{(L_1,1)}} \otimes \frac{\left(\mathbf{b}_l^{(L_2,2)}\right)^{\mathrm{H}}}{\left(\mathbf{b}_l^{(L_2,2)}\right)^{\mathrm{H}}\mathbf{b}_l^{(L_2,2)}} \otimes \\ &\frac{\left(\mathbf{b}_l^{(L_3,3)}\right)^{\mathrm{H}}}{\left(\mathbf{b}_l^{(L_3,3)}\right)^{\mathrm{H}}\mathbf{b}_l^{(L_3,3)}} \otimes \mathbf{I}_W \cdot \mathbf{V}^*\Sigma\mathbf{n}_l. \end{aligned} \tag{50}$$

Upon completing the tensor decomposition, we proceed to estimate the SCSI. Specifically, the SCSI $\{\bar{\tau}_{g,l}, \bar{\theta}_{g,l}, \bar{\varphi}_{g,l}, \bar{\rho}_{g,l}\}_{l=1}^{\bar{L}}$ can be estimated using the generators $\{z_{1,l}, z_{2,l}, z_{3,l}\}_{l=1}^{\bar{L}}$ and the factor matrix $\mathbf{B}^{(4)}$ as follows:

$$\bar{\tau}_{g,l} \triangleq -\frac{1}{2\pi\Delta f}\angle z_{1,l}, l = 1, \ldots, \bar{L}, \tag{51a}$$

$$\bar{\theta}_{g,l} \triangleq \arccos\left(-\frac{1}{\pi}\angle z_{2,l}\right), l = 1, \ldots, \bar{L}, \tag{51b}$$

$$\bar{\varphi}_{g,l} \triangleq \arccos\left(-\frac{1}{\pi\sin\bar{\theta}_{g,l}}\angle z_{3,l}\right), l = 1, \ldots, \bar{L}, \tag{51c}$$

$$\bar{\rho}_{l,g} \triangleq \frac{1}{W}\|\mathbf{b}_l^{(4)}\|_2^2, l = 1, \ldots, \bar{L}, \tag{51d}$$

where $\angle$ denotes the operator for extracting the phase angle. The VSTD-based SCSI database construction algorithm is summarized in Algorithm 2.

Algorithm 2 VSTD-Based SCSI Database Construction Algorithm for Grid g

Input: $\boldsymbol{\mathcal{H}}_g \in \mathbb{C}^{N_{\mathrm{d}} \times M_{\mathrm{v}} \times M_{\mathrm{h}} \times W}$

1: Compute $\mathbf{X}_{\mathcal{S}}$ using (36) and (37).
2: Compute the SVD of $\mathbf{X}_{\mathcal{S}}$ using (39).
3: Compute EVD as $\mathbf{U}_1^{\dagger}\mathbf{U}_2 = \mathbf{M}\mathbf{Z}_1\mathbf{M}^{-1}$.
4: Estimate the normalized generators $\{z_{1,l}, z_{2,l}, z_{3,l}\}_{l=1}^{\bar{L}}$ using (44)-(49).
5: Reconstruct $\left\{\mathbf{B}^{(1)}, \mathbf{B}^{(2)}, \mathbf{B}^{(3)}\right\}$ using $\{z_{1,l}, z_{2,l}, z_{3,l}\}_{l=1}^{\bar{L}}$.
6: Compute the factor matrices $\mathbf{B}^{(4)}$ using (50).
7: Compute $\left\{\bar{\tau}_{g,l}, \bar{\theta}_{g,l}, \bar{\varphi}_{g,l}, \bar{\rho}_{l,g}\right\}_{l=1}^{\bar{L}}$ via (51a) -(51d).

Output: $\{\bar{\tau}_{g,l}, \bar{\theta}_{g,l}, \bar{\varphi}_{g,l}, \bar{\rho}_{g,l}\}_{l=1}^{\bar{L}}$.

V. Simulation Results

A. Simulation Configuration

In this section, we present simulation results to evaluate the performance of the proposed algorithms. To generate the channels for simulations in the 3GPP 38.901 urban macro (UMa) line-of-sight (LOS) scenario, we utilize QuaDRiGa [52], which is capable of generating massive MIMO-OFDM channels that consistent with the 3GPP 38.901 specifications [53]. Each channel consists of 34 clusters, comprising 221 subpaths. Furthermore, the channel parameters vary at different positions in accordance with the spatial consistency procedure [53]. The basic simulation parameters are presented in Table I. Unless otherwise specified, a velocity of 0.1 km/h is adopted to focus on the impact of frequency-selective fading on the frequency-domain OCC decomposition, with additional simulations provided for high-mobility scenarios. Finally, the SNR during channel estimation and the location-specific SCSI database construction are denoted as $\mathrm{SNR}_{\mathrm{CE}}$ and $\mathrm{SNR}_{\mathrm{SC}}$, respectively.

B. Benchmarks and Performance Metric

To demonstrate the superiority of the proposed scheme, we compare our schemes with the following state-of-the-art algorithms:

- OMP without SCSI Database [54]: The orthogonal matching pursuit (OMP) algorithm estimates delay-angular channel parameters by applying OMP with a pre-defined dictionary from the trivial approach results [11]. The channel is subsequently reconstructed using the estimated parameters.
- VSD without SCSI Database [10]: The Vandermonde structured decomposition (VSD) algorithm exploits the

TABLE I: Basic System Parameters

System Parameters	Value
Centering frequency f_{c}	6.7 GHz
Bandwidth B	100 MHz
FFT size N_{FFT}	4096
Number of subcarriers for transmission N_{c}	816
Subcarrier spacing Δf	30 kHz
Number of CDM group G	3
Number of OFDM symbols for pilots T_{p}	2
Number of subcarriers each CDM group N	272
Number of UE K	24
Number of spatial sampling points W	10
Number of BS antennas $[M_{\mathrm{v}}, M_{\mathrm{h}}]$	[4,16]
Height of BS h_{BS}	25 m
Height of UE h_{UE}	1.5m
Delay spread	300ns
Shape parameter of the Kaiser window	3.95
Window function of SA-WBCE	Kaiser window
Bandsizes in SA-WBCE $[B_\tau, B_\phi]$	$[15, 20]$

channel's inherent Vandermonde structure, applying tensor decomposition to estimate the channel from the trivial approach results [11].

- EM-AMP without SCSI Database [20]: This algorithm assumes an unknown Bernoulli-Gaussian prior, learns the hyper-parameters through EM algorithm, and estimates the frequency-space domain channels of all users via approximate message passing (AMP) based on the trivial approach results.
- SA-BCE with SOMP-based SCSl Database: This algorithm leverages the SCSI database constructed via the simultaneous orthogonal matching pursuit (SOMP) algorithm for SA-BCE. The SOMP algorithm [55] extracts the SCSI under signal model (28), taking into account the common statistical properties of the channel across different spatial sampling points.

To evaluate the performance of SCSI database construction, we use the mean square error (MSE) of location-specific SCSI-assisted MMSE estimator as the performance metric, i.e.,

$$\mathcal{L}_{\mathrm{SCSI}} = \frac{\mathcal{E}_{\mathrm{f}} + \mathcal{E}_{\mathrm{s}}}{2}, \tag{52}$$

where $\mathcal{E}_{\mathrm{f}}$ and $\mathcal{E}_{\mathrm{s}}$ denote the MSE of the frequency-domain MMSE channel estimator and antenna-domain MMSE channel estimator, respectively, which can be expressed as

$$\begin{aligned} \mathcal{E}_{\mathrm{f}} &= \frac{1}{N_d} \operatorname{tr}\left(\mathbf{R}_{\mathrm{f}} - \mathbf{R}_{\mathrm{f}} \tilde{\mathbf{R}}_{\mathrm{f}} \left(\tilde{\mathbf{R}}_{\mathrm{f}} + \sigma^2 \mathbf{I}_N \right)^{-1} \right), \\ \mathcal{E}_{\mathrm{s}} &= \frac{1}{M} \operatorname{tr}\left(\mathbf{R}_{\mathrm{s}} - \mathbf{R}_{\mathrm{s}} \tilde{\mathbf{R}}_{\mathrm{s}} \left(\tilde{\mathbf{R}}_{\mathrm{s}} + \sigma^2 \mathbf{I}_M \right)^{-1} \right), \end{aligned} \tag{53}$$

where $\mathbf{R}_{\mathrm{f}} \in \mathbb{C}^{N_{\mathrm{c}} \times N_{\mathrm{c}}}$ and $\mathbf{R}_{\mathrm{s}} \in \mathbb{C}^{M \times M}$ denote the ideal frequency-domain and antenna-domain channel correlation matrices, respectively, $\tilde{\mathbf{R}}_{\mathrm{f}} \in \mathbb{C}^{N_{\mathrm{c}} \times N_{\mathrm{c}}}$ and $\tilde{\mathbf{R}}_{\mathrm{s}} \in \mathbb{C}^{M \times M}$ represent the frequency-domain and antenna-domain channel covariance matrices obtained using the SCSI from location-specific SCSI database.

To assess the performance of channel estimation, we introduce the normalized mean squared error (NMSE) as the evaluation metric, i.e.,

$$\mathrm{NMSE} = \frac{1}{T_p K} \sum_{k=1}^{K} \sum_{t=1}^{T_p} 10 \log_{10} \left(\frac{\|\hat{\mathbf{H}}_k(t) - \mathbf{H}_k(t)\|_{\mathrm{F}}^2}{\|\mathbf{H}_k(t)\|_{\mathrm{F}}^2} \right), \tag{54}$$

where $\mathbf{H}_k(t) \in \mathbb{C}^{N_{\mathrm{c}} \times M}$ and $\hat{\mathbf{H}}_k(t) \in \mathbb{C}^{N_{\mathrm{c}} \times M}$ represent the actual and estimated frequency-space domain channel for the k-th user at the t-th symbol duration.

TABLE II: Computational Complexity of VSTD Algorithm

Main Steps	Computational Complexity
Perform truncated SVD on $\mathbf{X}_{\mathcal{S}}$	$\mathcal{O}\left(K_1 L_1 K_2 L_2 K_3 L_3 W \bar{L}\right)$
Perform EVD on $\mathbf{U}_1^{\dagger}\mathbf{U}_2$	$\mathcal{O}\left(K_1 K_2 K_3 \bar{L}^2\right)$
Compute $\{z_{2,l}\}_{l=1}^{\bar{L}}$	$\mathcal{O}\left(K_1 K_2 K_3 \bar{L}^2\right)$
Compute $\{z_{3,l}\}_{l=1}^{\bar{L}}$	$\mathcal{O}\left(K_2 K_3 \bar{L}\right)$
Reconstruct $\mathbf{B}^{(4)}$	$\mathcal{O}\left(L_1 L_2 L_3 W \bar{L}^2\right)$
Total	$\mathcal{O}\left(K_1 L_1 K_2 L_2 K_3 L_3 W \bar{L}\right)$

C. Computational Complexity

1) Location-specific SCSI database construction: Since the process of constructing the matrix $\mathbf{X}_{\mathcal{S}}$ by collecting specific rows incurs negligible cost, the overall computational complexity of the VSTD algorithm can be decomposed into four steps, as summarized in Table II. Among these steps, the truncated SVD performed on $\mathbf{X}_{\mathcal{S}}$ is the dominant component, with a complexity of $\mathcal{O}\left(K_1 L_1 K_2 L_2 K_3 L_3 W \bar{L}\right)$. In contrast, the primary operations in SOMP involve searching for the matched steering vectors $\mathbf{b}_{N_{\mathrm{d}}}(\cdot) \otimes \mathbf{a}_{\mathrm{v}}(\cdot) \otimes \mathbf{a}_{\mathrm{h}}(\cdot) \in \mathbb{C}^{N_{\mathrm{d}} M \times 1}$ and performing a LS estimation of the matrix $\mathbf{B}^{(4)} \in \mathbb{C}^{W \times \bar{L}}$, resulting in a computational complexity of $\mathcal{O}\left(N_{\mathrm{d}}^2 M^2 W \bar{L} + \bar{L}^3\right)$. By exploiting the tensor-structured characteristics of wireless channels, the proposed VSTD algorithm avoids high-dimensional matrix operations, thereby achieving lower computational complexity and improved performance compared to SOMP. Furthermore, to evaluate scalability with respect to both the antenna array size and the system bandwidth, we analyze the multiplication counts of both algorithms under varying antenna configurations and subcarrier numbers, as summarized in Table III. The results demonstrate that the VSTD algorithm exhibits favorable scalability in both cases, thereby underscoring its computational efficiency and suitability for large-scale wideband massive MIMO systems.

2) Channel estimation: In SA-BCE, the primary computational cost originates from matrix inversions and multiplications. To alleviate the computational burden of matrix inversion, we implement SA-BCE in the beam-delay domain and employ a windowing technique, which simplifies the matrix inversion in SA-BCE to the inversion of band matrices in SA-WBCE. Furthermore, in both SA-BCE and SA-WBCE, the frequency-domain MMSE estimator requires matrix inversion to be performed once per CDM group. The computational complexity of the proposed algorithms and baselines is summarized in Table IV, where L denotes the number of iterations in OMP, R represents the predefined tensor rank in VSD, T_{iter} denotes the number of iterations in the EM-AMP algorithm. In general, both L and R are set as the maximum number of effective channel paths.

TABLE III: Multiplication counts of VSTD and SOMP algorithms under varying antenna array sizes and subcarrier numbers

Algorithm	Multiplication Count					
	$[M_{\mathrm{v}}, M_{\mathrm{h}}] = [4, 16]$	$[M_{\mathrm{v}}, M_{\mathrm{h}}] = [16, 16]$	$[M_{\mathrm{v}}, M_{\mathrm{h}}] = [16, 32]$	$N_{\mathrm{d}} = 240$	$N_{\mathrm{d}} = 480$	$N_{\mathrm{d}} = 960$
VSTD	5.25×10^9	6.09×10^{10}	2.29×10^{11}	5.25×10^9	2.04×10^{10}	8.07×10^{10}
SOMP	1.89×10^{11}	3.02×10^{12}	1.21×10^{13}	1.89×10^{11}	7.55×10^{11}	3.02×10^{12}

TABLE IV: Computational Complexity of Channel Estimation Methods

Algorithm	Computational Complexity
OMP	$\mathcal{O}\left(K\left(N^2M^2L + L^3\right)\right)$
VSD	$\mathcal{O}(KN^2M^2R)$
EM-AMP	$\mathcal{O}\left(KN^2M^2T_{\text{iter}}\right)$
SA-BCE	$\mathcal{O}\left(G\left(N^3 + N^2M\right) + KN^2M\right) + \mathcal{O}\left(KM^3 + KNM^2\right)$
SA-WBCE	$\mathcal{O}\left(G\left(NB_\tau^2 + N^2M\right) + KN^2M\right) + \mathcal{O}\left(KMB_\phi^2 + KNM^2\right)$

As shown in Table IV, the proposed SA-BCE and SA-WBCE schemes achieve lower computational complexity than baseline methods that jointly process signals in the antenna-frequency domain. This reduction is enabled by leveraging location-specific SCSI and decoupling processing across frequency and antenna domains. In addition to the asymptotic complexity summarized in Table IV, we further report the multiplication counts under different antenna array sizes and numbers of subcarriers in Table V, which serve as a more quantitative metric of computational burden. The results confirm that the proposed SA-BCE and SA-WBCE schemes achieve substantially better scalability than the baseline algorithms, whose complexity grows quadratically. In particular, SA-WBCE attains strictly sub-quadratic scaling by replacing full matrix inversion with band-matrix inversion, thereby ensuring computational feasibility for large-scale massive MIMO deployments.

D. Performance Evaluation

The SCSI accuracy of the proposed VSTD-based algorithm compared to the SOMP-based benchmark under varying SNR and N_{d} is depicted in Fig. 3. It is evident that the proposed algorithm consistently enhances SCSI accuracy with increases in both N_{d} and SNR. Across the entire evaluated range of N_{d}, the VSTD-based SCSI database construction algorithm demonstrates substantial superiority over the SOMP-based baseline. To quantify, at $N_{\mathrm{d}} = 180$ and an $\mathrm{SNR}_{\mathrm{SC}}$ of 10 dB, the proposed algorithm realizes a SCSI accuracy of -23.5 dB, which is 16.3 dB superior to the -7.2 dB achieved by the SOMP-based approach.

Fig. 4 presents the SCSI accuracy of the proposed algorithm as a function of the grid size d and the number of subcarriers N_{d}. The proposed algorithm exhibits an improvement in SCSI accuracy with an increase in N_{d} or a decrease in d. Notably, to maintain a consistent SCSI accuracy of -23.4 dB, an increase in the grid size d from 2 m to 5 m necessitates a substantial increase in N_{d}, specifically from 120 to 240. This observation highlights a critical trade-off: while smaller grid sizes enhance SCSI accuracy, they lead to finer grid partitioning and consequently increase the storage overhead

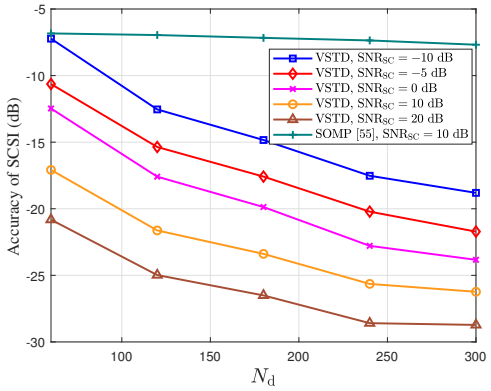

Fig. 3: SCSI accuracy versus N_{d} ($d = 2$m, $\sigma^2 = 10^{-3}$).

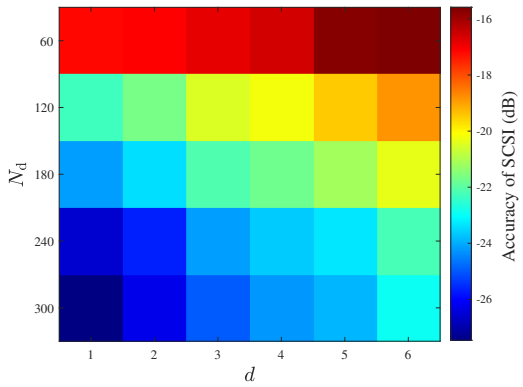

Fig. 4: The SCSI accuracy of the VSTD-based SCSI database at different N_{d} and d ($\mathrm{SNR}_{\mathrm{SC}} = 10$ dB, $\sigma^2 = 10^{-3}$).

for the SCSI database. Thus, a judicious selection of d is imperative to achieve an optimal balance between accuracy and storage efficiency.

The sensitivity of the proposed SA-BCE and SA-WBCE schemes to the grid size in location-specific SCSI acquisition is evaluated in Fig. 5. It can be observed that although increasing the grid size leads to performance degradations for both SA-BCE and SA-WBCE, the gaps are relatively small. This is because, although larger grids result in coarser user position quantization and reduced accuracy of the retrieved SCSI, essential channel characteristics, such as angle and delay spectra, are still effectively preserved due to spatial consistency, leading to only marginal performance degradation. Specifically, when the grid size grows from 2m to 10m, the performance losses are only about 2 dB for SA-BCE and 2.5 dB for SA-WBCE. These observations indicate that the proposed methods exhibit strong robustness to grid size, allowing the storage overhead of the SCSI database to be significantly reduced by enlarging the grid size with only a marginal performance degradation.

TABLE V: Multiplication counts of channel estimation algorithms under varying antenna array sizes and subcarrier numbers

Algorithm	Multiplication Count					
	$[M_{\mathrm{v}}, M_{\mathrm{h}}] = [4, 16]$	$[M_{\mathrm{v}}, M_{\mathrm{h}}] = [16, 16]$	$[M_{\mathrm{v}}, M_{\mathrm{h}}] = [16, 32]$	$N_{\mathrm{c}} = 816$	$N_{\mathrm{c}} = 1632$	$N_{\mathrm{c}} = 3264$
SA-BCE	2.21×10^8	1.40×10^9	6.01×10^9	2.21×10^8	1.05×10^9	6.02×10^9
SA-WBCE	1.55×10^8	9.79×10^8	3.04×10^9	1.55×10^8	5.66×10^8	2.15×10^9
OMP	5.82×10^{11}	9.31×10^{12}	3.72×10^{13}	5.82×10^{11}	2.33×10^{12}	9.31×10^{12}
VSD	5.82×10^{11}	9.31×10^{12}	3.72×10^{13}	5.82×10^{11}	2.33×10^{12}	9.31×10^{12}
EM-AMP	2.18×10^{12}	3.49×10^{13}	1.40×10^{14}	2.18×10^{12}	8.73×10^{12}	3.49×10^{13}

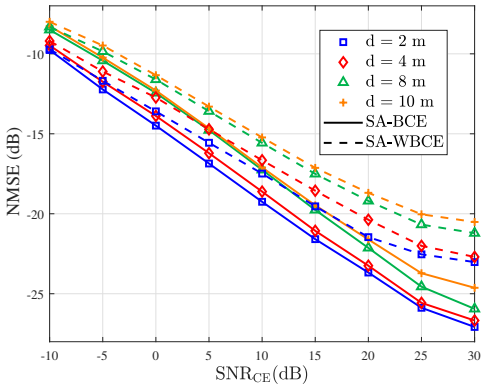

Fig. 5: The NMSE performance of the proposed SA-BCE and SA-WBCE schemes with different grid size d ($N_{\mathrm{d}} = 240$ and $\mathrm{SNR}_{\mathrm{SC}} = 10$ dB in SCSI database construction).

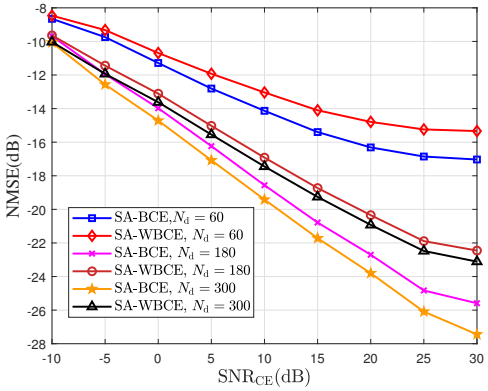

Fig. 6: The NMSE of the proposed methods with different N_{d} in SCSI database construction ($d = 2$ m and $\mathrm{SNR}_{\mathrm{SC}} = 10$ dB in SCSI database construction).

To examine how the channel estimation performance of the proposed method varies with the number of subcarriers used for location-specific SCSI acquisition, we present NMSE performance for the proposed SA-BCE and SA-WBCE method with different N_{d} in Fig. 6. As shown in the figure, the performance of the proposed algorithm improves with the increasing SNR. Furthermore, the performance of the proposed algorithm improves as N_{d} increases. When N_{d} is small, the condition in (35) may not be satisfied, leading to inaccurate SCSI and degraded channel estimation performance. When N_{d} is large, increasing N_{d} does not significantly improve the channel estimation performance. Therefore, during the construction of the SCSI database, only a subset of measurement data is required. Furthermore, the SA-WBCE exhibits inferior performance compared to SA-BCE, particularly in the high-SNR regime. This result stems from the approximations made during the design process, which, in turn, contribute to a significant reduction in computational complexity.

The comparison of NMSE and average effective communication rate performance between the proposed schemes and baseline methods is shown in Fig. 7. By leveraging the SCSI, the proposed schemes outperform all benchmark methods across the entire SNR range and achieves performance comparable to the SA-BCE with the ideal SCSI database. In particular, the proposed SA-BCE and SA-WBCE with the VSTD-based SCSI database achieve an NMSE of approximately -21.5 dB and -19.5 dB when SNR is 15 dB, whereas the NMSE of all other benchmark methods remains above -17 dB. These results demonstrate the great potential of the proposed SA-BCE and SA-WBCE for MU-MIMO systems.

Fig. 8 illustrates the NMSE performance of the SA-WBCE with the VSTD-based SCSI database under different band sizes and window functions. As the band size increases, the NMSE performance of the SA-WBCE scheme improves, albeit at the cost of higher computational complexity. In practical applications, a trade-off between performance and complexity can be achieved by appropriately selecting the band size. Among the three window functions, the Kaiser window offers the best performance. Specifically, When $B_\tau = 15$ and $B_a = 20$, the SA-WBCE with the Kaiser window achieves an NMSE of -21.4 dB, representing a 2 dB improvement than SA-WBCE with the rectangular window.

In Fig. 9, we present the NMSE performance of various algorithms as a function of the channel delay spread. The OMP, VSD, and EM-AMP algorithms, which rely on OCC decomposition results obtained through trivial approach for channel estimation, suffer significant performance degradation as the delay spread increases. In contrast, the proposed SA-BCE and SA-WBCE, which incorporate SCSI into the OCC decomposition process to mitigate pilot interference, exhibit minimal NMSE deterioration. Specifically, as the delay spread increases from 200 ns to 500 ns, the proposed algorithms experiences only a 0.5 dB NMSE loss, compared to a 6.5 dB degradation observed in the VSD and EM-AMP algorithms.

The NMSE performance of the several schemes with respect to user mobility is depicted in Fig. 10. As observed, increasing the user speed leads to only a marginal NMSE degradation across all methods, with the proposed SA-BCE and SA-WBCE schemes consistently outperforming the baseline approaches. The negligible performance loss is mainly attributed to the DMRS patterns defined in the specifications [9] [56]. In OFDM systems, Doppler frequency mainly induces phase rotation between successive symbols. Since DMRS spans two consecutive OFDM symbols, the resulting phase

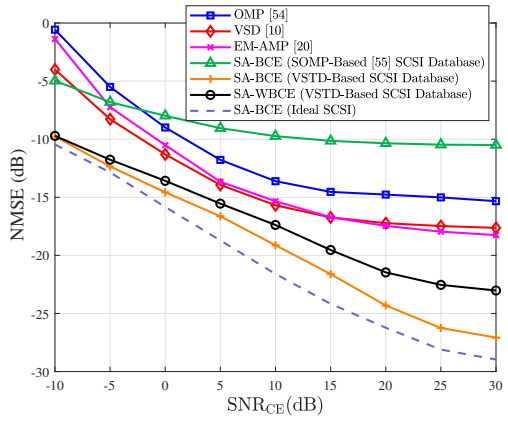

(a) NMSE

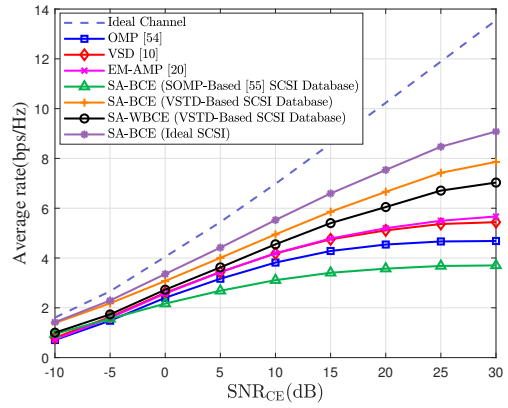

(b) Average effective communication rate

Fig. 7: The NMSE and average effective communication rate performance versus SNR ($N_{\mathrm{d}} = 240$, $\mathrm{SNR}_{\mathrm{SC}} = 10$ dB and $d = 2$m in SCSI database construction).

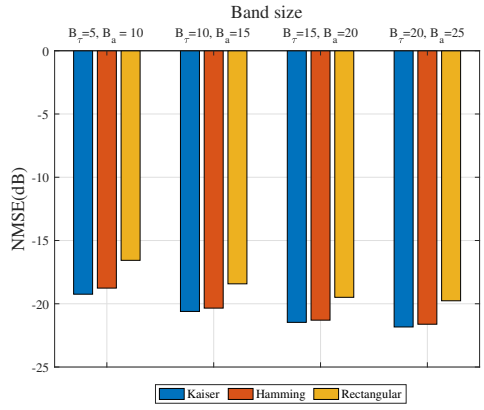

Fig. 8: The NMSE performance of the SA-WBCE with different band size and different window functions ($N_{\mathrm{d}} = 240$, $\mathrm{SNR}_{\mathrm{SC}} = 10$dB and $d = 2$m in SCSI database construction, $\mathrm{SNR}_{\mathrm{CE}} = 20$dB).

rotation is limited, thereby preserving the orthogonality in time-domain OCC decomposition. In contrast, as illustrated in Fig. 9, the frequency-domain OCC decomposition is more susceptible to delay spread because the widely spaced DMRS subcarriers within each CDM group experience distinct fading, breaking orthogonality and consequently degrading NMSE performance.

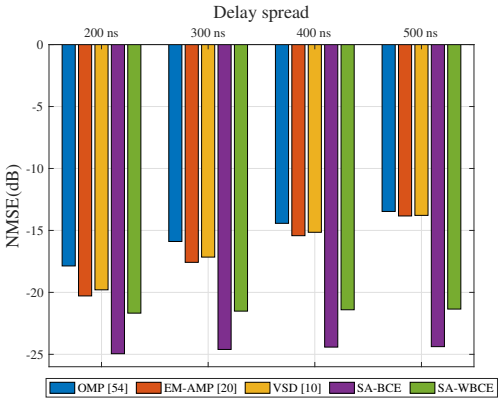

Fig. 9: The NMSE performance of several schemes versus the delay spread ($N_{\mathrm{d}} = 240$, $\mathrm{SNR}_{\mathrm{SC}} = 10$dB and $d = 2$m in SCSI database construction, $\mathrm{SNR}_{\mathrm{CE}} = 20$dB).

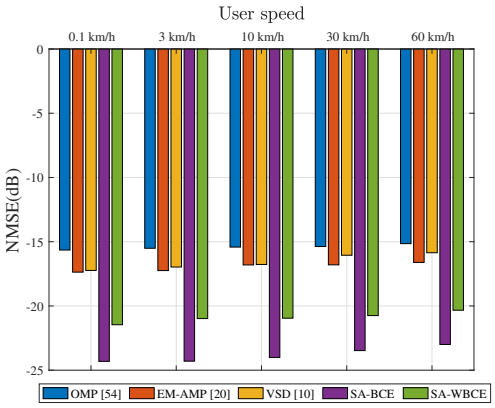

Fig. 10: The NMSE performance of several schemes versus the user speed($N_{\mathrm{d}} = 240, \mathrm{SNR}_{\mathrm{SC}} = 10$ dB and $d = 2$ m in SCSI database construction, $\mathrm{SNR}_{\mathrm{CE}} = 20$ dB).

In future wireless communication systems, both antenna array size and system bandwidth are expected to scale up significantly, necessitating an evaluation of the proposed schemes under such configurations. Fig. 11 presents the NMSE results with varying numbers of BS antennas and subcarriers. In both cases, the proposed SA-BCE and SA-WBCE consistently achieve the lowest NMSE among all baselines. This is because the estimation accuracy is highly determined by the spatial and delay-domain resolutions which are governed by the antenna array size and system bandwidth, respectively. Increasing the antenna array size and system bandwidth enhances these resolutions, enabling more effective separation of multipath components and reducing energy leakage. However, as the antenna array size or system bandwidth increases beyond a certain threshold, the dominant propagation paths become sufficiently distinguishable, leading to diminishing returns in channel estimation accuracy and resulting in only marginal NMSE improvements.

In practical localization systems [37], non-negligible positioning errors are inevitable. Moreover, in high-mobility scenarios, the localization and database access latency may further exacerbate user location errors. To assess the impact of such errors, Fig. 12 illustrates the NMSE performance of

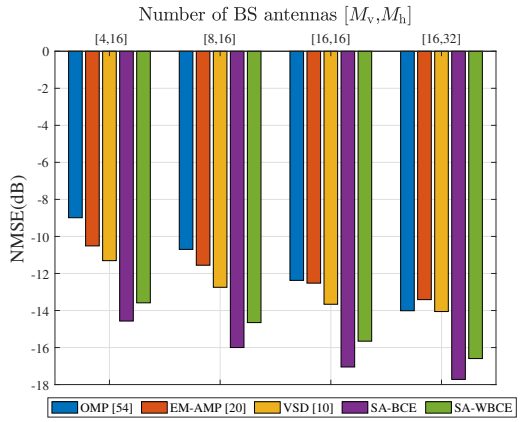

(a) Lager antenna arrays

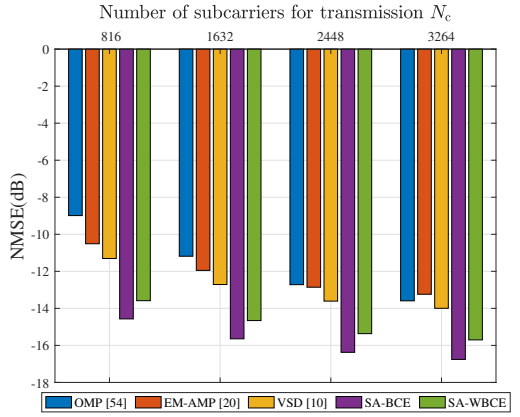

(b) Wider bandwidths

Fig. 11: NMSE performance of several schemes versus: (a) the number of BS antennas $[M_v, M_h]$; and (b) the number of subcarriers N_c ($N_d = 240, \mathrm{SNR}_{SC} = 10$ dB, $d = 2$ m in SCSI database construction; $\mathrm{SNR}_{CE} = 0$ dB).

SA-BCE and SA-WBCE under different levels of location error. The results indicate that NMSE degrades gradually as the error increases, due to the potential mismatch between the estimated user position and the true grid location, which leads to erroneous SCSI retrieval. With a location error of 2 m, the resulting performance degradation is relatively minor, with an NMSE increase of approximately 1 dB. As the error increases to 6 m and 10 m, the degradation becomes more pronounced, reaching about 3 dB and 4 dB, respectively. For small errors (up to 4 m), the proposed methods maintain a clear performance advantage over all baseline methods across the entire SNR range. In scenarios with larger location errors, the proposed schemes still deliver competitive performance, and their robustness can be further enhanced by increasing the grid size. This adjustment effectively mitigates the impact of position mismatch and helps maintain consistent performance across different SNR levels, as demonstrated in Fig. 5.

VI. Conclusion

In this paper, we investigated uplink DMRS-based channel estimation for MU-MIMO systems. We first developed the received signal model under the Type II OCC pattern

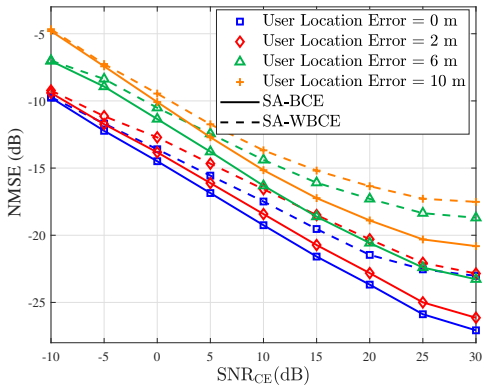

Fig. 12: The NMSE performance of the proposed SA-BCE and SA-WBCE schemes with different user location errors ($N_d = 240, \mathrm{SNR}_{SC} = 10$ dB and $d = 2$ m in SCSI database construction).

standardized in 3GPP Release 18. Building on this model, we proposed SA-BCE, which effectively suppresses pilot interference by fully leveraging SCSI. To further reduce the computational complexity of SA-BCE, we reformulated the estimation process from the antenna-frequency domain to the beam-delay domain and extended the approach to SA-WBCE by incorporating the windowing technique. To acquire SCSI, we constructed a location-specific SCSI database by partitioning the spatial region into grids and leveraged the uplink received signals within each grid to extract the SCSI. Facilitated by the multilinear structure of wireless channels, we formulated the SCSI acquisition problem within each grid as a tensor decomposition problem and exploited the VSTD algorithm to extract the SCSI. Simulation results validated the superiority of the proposed schemes. In future work, we plan to extend the proposed framework to more practical settings, including dynamic environments with moving scatterers and scenarios affected by pilot contamination.

References

[1] J. Zhuang, H. Hou, M. Tang, W. Wang, S. Jin, and V. K. Lau, "A Bayesian approach to windowed DMRS channel estimation for uplink MU-MIMO systems," in *Proc. IEEE GLOBECOM Workshops (GC Wkshps)*, Taipei, Taiwan, Dec. 2025.

[2] H. Zhou, Y. Deng, and A. Nallanathan, "Novel listen-before-talk access scheme with adaptive backoff procedure for uplink centric broadband communication," *IEEE Internet Things J.*, vol. 10, no. 22, pp. 19 981–19 992, Nov. 2023.

[3] F. Hu, Y. Deng, H. Zhou, T. H. Jung, C.-B. Chae, and A. H. Aghvami, "A vision of an XR-aided teleoperation system toward 5G/B5G," *IEEE Commun. Mag.*, vol. 59, no. 1, pp. 34–40, Jan. 2021.

[4] "Huawei's David Wang: Defining 5.5G for a better, intelligent world." Nov. 2020. [Online]. Available: https://www.huawei.com/en/news/2020/11/mbbf-shanghai-huawei-david-wang-5dot5g.

[5] W. Chen, X. Lin, J. Lee, A. Toskala, S. Sun, C. F. Chiasserini, and L. Liu, "5G-advanced toward 6G: Past, present, and future," *IEEE J. Sel. Areas Commun.*, vol. 41, no. 6, pp. 1592–1619, Jun. 2023.

[6] X. Lin, "An overview of 5G advanced evolution in 3GPP release 18," *IEEE Commun. Stand. Mag.*, vol. 6, no. 3, pp. 77–83, Sep. 2022.

[7] Y. Wang, H. Hou, X. Yi, W. Wang, and S. Jin, "Towards unified AI models for MU-MIMO communications: A tensor equivariance framework," *IEEE Trans. Wireless Commun.*, Jul. 2025, Early Access.

[8] Y. Wang, H. Hou, W. Wang, X. Yi, and S. Jin, "Soft demodulator for symbol-level precoding in coded multiuser MISO systems," *IEEE Trans. Wireless Commun.*, vol. 23, no. 10, pp. 14 819–14 835, Oct. 2024.

[9] *Physical channels and modulation, Version 18.4.0*. Standard 3GPP T.R. 38.211, Sep. 2024.

[10] P. Chen and L. Cheng, "Estimating channels with hundreds of sub-paths for MU-MIMO uplink: A structured high-rank tensor approach," *IEEE Signal Process. Lett.*, vol. 31, pp. 2320–2324, Sep. 2024.

[11] U. Mutlu and Y. Kabalci, "Deep learning aided channel estimation approach for 5G communication systems," in *2022 4th Global Power, Energy and Communication Conference (GPECOM)*. IEEE, 2022, pp. 655–660.

[12] D. Kong, X.-G. Xia, P. Liu, and Q. Zhu, "MMSE channel estimation for two-port demodulation reference signals in new radio," *arXiv preprint arXiv:2007.14168*, 2020.

[13] C. Sun, X. Gao, S. Jin, M. Matthaiou, Z. Ding, and C. Xiao, "Beam division multiple access transmission for massive MIMO communications," *IEEE Trans. Commun.*, vol. 63, no. 6, pp. 2170–2184, Jun. 2015.

[14] D. Han, J. Park, and N. Lee, "FDD massive MIMO without CSI feedback," *IEEE Trans. Wireless Commun.*, vol. 23, no. 5, pp. 4518–4530, May 2024.

[15] C. Cai, J. Yang, F. Yang, and X. Gao, "Expectation-maximization-based information geometry approach for massive MIMO-OFDM channel estimation," *IEEE Trans. Commun.*, vol. 73, no. 8, pp. 6366–6378, Aug. 2025.

[16] Y. Zhu, J. Zhuang, G. Sun, H. Hou, L. You, and W. Wang, "Joint channel estimation and prediction for massive MIMO with frequency hopping sounding," *IEEE Trans. Commun.*, vol. 73, no. 7, pp. 5139–5154, Jul. 2025.

[17] S. Cai, L. Chen, Y. Chen, H. Yin, and W. Wang, "Joint channel estimation and data recovery for millimeter massive MIMO: Using pilot to capture principal components," *IEEE Trans. Commun.*, vol. 73, no. 2, pp. 781–799, Feb. 2025.

[18] Y. Wan and A. Liu, "A two-stage 2D channel extrapolation scheme for TDD 5G NR systems," *IEEE Trans. Wireless Commun.*, vol. 23, no. 8, pp. 8497–8511, Aug. 2024.

[19] A.-A. Lu, Y. Chen, and X. Gao, "2D beam domain statistical CSI estimation for massive MIMO uplink," *IEEE Trans. Wireless Commun.*, vol. 23, no. 1, pp. 749–761, Jan. 2023.

[20] J. P. Vila and P. Schniter, "Expectation-maximization Gaussian-mixture approximate message passing," *IEEE Trans. Signal Process.*, vol. 61, no. 19, pp. 4658–4672, Oct. 2013.

[21] Y. Zeng and X. Xu, "Toward environment-aware 6G communications via channel knowledge map," *IEEE Wireless Commun.*, vol. 28, no. 3, pp. 84–91, Jun. 2021.

[22] Y. Zeng, J. Chen, J. Xu, D. Wu, X. Xu, S. Jin, X. Gao, D. Gesbert, S. Cui, and R. Zhang, "A tutorial on environment-aware communications via channel knowledge map for 6G," *IEEE Commun. Surv. Tutor*, vol. 26, no. 3, pp. 1478–1519, Feb. 2024.

[23] X. Xu and Y. Zeng, "How much data is needed for channel knowledge map construction?" *IEEE Trans. Wireless Commun.*, vol. 23, no. 10, pp. 13 011–13 021, Oct. 2024.

[24] J. Chen, R. Gao, J. Wang, S. Sun, and Y. Wu, "Channel gain map construction based on subregional learning and prediction," *IEEE Trans. Veh. Technol.*, vol. 74, no. 6, pp. 9852–9857, Jun. 2025.

[25] Z. Jin, L. You, J. Wang, X.-G. Xia, and X. Gao, "An I2I inpainting approach for efficient channel knowledge map construction," *IEEE Trans. Wireless Commun.*, vol. 24, no. 2, pp. 1415–1429, Feb. 2025.

[26] C. Wu, X. Yi, Y. Zhu, W. Wang, L. You, and X. Gao, "Channel prediction in high-mobility massive MIMO: From spatio-temporal autoregression to deep learning," *IEEE J. Sel. Areas Commun.*, vol. 39, no. 7, pp. 1915–1930, Jul. 2021.

[27] W. Jiang, X. Yuan, B. Teng, H. Wang, and J. Qian, "Interference-cancellation-based channel knowledge map construction and its applications to channel estimation," *IEEE Trans. Wireless Commun.*, vol. 24, no. 7, pp. 6240–6256, Jul. 2025.

[28] D. Tse and P. Viswanath, *Fundamentals of Wireless Communication*. Cambridge university press, 2005.

[29] L. You, X. Gao, A. L. Swindlehurst, and W. Zhong, "Channel acquisition for massive MIMO-OFDM with adjustable phase shift pilots," *IEEE Trans. Signal Process.*, vol. 64, no. 6, pp. 1461–1476, Mar. 2016.

[30] S. M. Kay, *Fundamentals of Statistical Signal Processing: Estimation Theory*. Hoboken, NJ, USA: Prentice-Hall, Inc., 1993.

[31] R. He, B. Ai, G. Wang, M. Yang, C. Huang, and Z. Zhong, "Wireless channel sparsity: Measurement, analysis, and exploitation in estimation," *IEEE Wireless Commun. Mag.*, vol. 28, no. 4, pp. 113–119, Aug. 2021.

[32] P.-F. Cui, J. A. Zhang, W.-J. Lu, Y. J. Guo, and H. Zhu, "Statistical sparse channel modeling for measured and simulated wireless temporal channels," *IEEE Trans. Wireless Commun.*, vol. 18, no. 12, pp. 5868–5881, Dec. 2019.

[33] N. K. Jha, H. Guo, and V. K. N. Lau, "Bayesian deep end-to-end learning for MIMO-OFDM system with delay-domain sparse precoder," *arXiv preprint: 2504.20777*, 2025.

[34] X. Yu, X. Gao, A.-A. Lu, J. Zhang, H. Wu, and G. Y. Li, "Robust precoding for HF skywave massive MIMO," *IEEE Trans. Wireless Commun.*, vol. 22, no. 10, pp. 6691–6705, Oct. 2023.

[35] C. Cai, J. Yang, F. Yang, H. Wu, and X. Gao, "Windowed information geometry approach for low-complexity channel estimation in massive MIMO-OFDM systems," *IEEE Trans. Wireless Commun.*, vol. 24, no. 1, pp. 244–259, Jan. 2025.

[36] L. Song, D. Shi, X. Gao, G. Y. Li, and X.-G. Xia, "Beam structured turbo receiver for HF skywave massive MIMO," *arXiv preprint arXiv:2501.07041*, 2025.

[37] F. Liu, Y. Cui, C. Masouros, J. Xu, T. X. Han, Y. C. Eldar, and S. Buzzi, "Integrated sensing and communications: Toward dual-functional wireless networks for 6G and beyond," *IEEE J. Sel. Areas Commun.*, vol. 40, no. 6, pp. 1728–1767, Jun. 2022.

[38] F. Xiao, Z. Zhao, and D. T. M. Slock, "Multipath component power delay profile based ranging," *IEEE J. Sel. Top. Signal Process.*, vol. 18, no. 5, pp. 950–963, Jul. 2024.

[39] C. Wu, Y. Zhu, W. Wang, C.-X. Wang, and X. Gao, "Improvement of the cluster-level spatial consistency of channel simulator with reference points transition method," *IEEE Trans. Veh. Technol.*, vol. 71, no. 6, pp. 5867–5879, Jun. 2022.

[40] 3GPP, "Technical specification group radio access network; study on NR positioning enhancements," 3GPP, TR 38.857, 2021, release 17.

[41] L. Italiano, B. C. Tedeschini, M. Brambilla, H. Huang, M. Nicoli, and H. Wymeersch, "A tutorial on 5G positioning," *arXiv preprint arXiv:2311.10551*, 2023.

[42] Y. Ruan, L. Chen, X. Zhou, G. Guo, and R. Chen, "Hi-loc: Hybrid indoor localization via enhanced 5G NR CSI," *IEEE Trans. Instrum. Meas.*, vol. 71, pp. 1–15, 2022.

[43] B. C. Tedeschini, G. Kwon, M. Nicoli, and M. Z. Win, "Real-time bayesian neural networks for 6G cooperative positioning and tracking," *IEEE J. Sel. Areas Commun.*, vol. 42, no. 9, pp. 2322–2338, Sep. 2024.

[44] H. Hou, Y. Wang, Y. Zhu, X. Yi, W. Wang, D. Slock, and S. Jin, "A tensor-structured approach to dynamic channel prediction for massive MIMO systems with temporal non-stationarity," *arXiv preprint arXiv:2412.06713*, 2024.

[45] H. Hou, Y. Wang, X. Yi, W. Wang, D. Slock, and S. Jin, "Tensor-structured Bayesian channel prediction for upper mid-band XL-MIMO systems," *arXiv preprint arXiv:2508.08491*, 2025.

[46] N. D. Sidiropoulos, L. De Lathauwer, X. Fu, K. Huang, E. E. Papalexakis, and C. Faloutsos, "Tensor decomposition for signal processing and machine learning," *IEEE Trans. Signal Process.*, vol. 65, no. 13, pp. 3551–3582, Jul. 2017.

[47] P. Comon, X. Luciani, and A. L. De Almeida, "Tensor decompositions, alternating least squares and other tales," *J. Chemometrics: A J. Chemometrics Soc.*, vol. 23, no. 7-8, pp. 393–405, Apr. 2009.

[48] J. B. Kruskal, "Three-way arrays: rank and uniqueness of trilinear decompositions, with application to arithmetic complexity and statistics," *Linear Algebra Appl.*, vol. 18, no. 2, pp. 95–138, 1977.

[49] M. Sørensen and L. De Lathauwer, "Blind signal separation via tensor decomposition with Vandermonde factor: Canonical polyadic decomposition," *IEEE Trans. Signal Process.*, vol. 61, no. 22, pp. 5507–5519, Nov. 2013.

[50] X. Liu and N. D. Sidiropoulos, "Almost sure identifiability of constant modulus multidimensional harmonic retrieval," *IEEE Trans. Signal Process.*, vol. 50, no. 9, pp. 2366–2368, Sep. 2002.

[51] K. Liu, J. P. C. Da Costa, H. C. So, L. Huang, and J. Ye, "Detection of number of components in CANDECOMP/PARAFAC models via minimum description length," *Digit. Signal Process.*, vol. 51, pp. 110–123, Jan. 2016.

[52] S. Jaeckel, L. Raschkowski, K. Börner, and L. Thiele, "QuaDRiGa: A 3-D multi-cell channel model with time evolution for enabling virtual field trials," *IEEE Trans. Antennas Propagat.*, vol. 62, no. 6, pp. 3242–3256, Jun. 2014.

[53] *Study on channel model for frequencies from 0.5 to 100 GHz, Version 16.1.0*. document 3GPP T.R. 38.901, Dec. 2019.

[54] J. A. Tropp and A. C. Gilbert, "Signal recovery from random measurements via orthogonal matching pursuit," *IEEE Trans. Inf. Theory*, vol. 53, no. 12, pp. 4655–4666, Dec. 2007.

[55] J.-F. Determe, J. Louveaux, L. Jacques, and F. Horlin, "On the exact recovery condition of simultaneous orthogonal matching pursuit," *IEEE Signal Process. Lett.*, vol. 23, no. 1, pp. 164–168, Jan. 2015.
[56] *NR, Physical channels and modulation, Version 16.6.0*. Standard 3GPP T.S. 38.211, Jun. 2021.

Jiawei Zhuang (Graduate Student Member, IEEE) received the B.E. degree in information engineering from Southeast University, Nanjing, China, in 2023. He is currently pursuing the Ph.D. degree with the National Mobile Communications Research Laboratory, Southeast University, Nanjing, China. His research interests are mainly on massive MIMO communications, signal processing, and channel estimation.

Hongwei Hou (Graduate Student Member, IEEE) received the B.E. degree in information engineering from Southeast University, Nanjing, China, in 2020. He is currently pursuing the Ph.D. degree with the National Mobile Communications Research Laboratory, Southeast University, Nanjing, China. From 2024 to 2025, he was a visiting Ph.D. student at the Communication Systems Department, EURECOM, France. His research interests are mainly on massive MIMO communications, statistical signal processing, and deep learning.

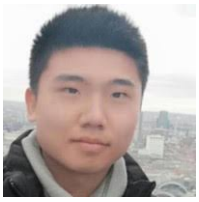

Minjie Tang (Member, IEEE) received the B.Eng. degree in information and communication engineering from The Huazhong University of Science and Technology (HUST), Wuhan, China, in 2018, and the Ph.D. degree in electronic and computer engineering from The Hong Kong University of Science and Technology (HKUST), Hong Kong, in 2024. He is currently a Postdoctoral Research Fellow at Communication Systems Department, EURECOM, France. His current research interests include semantic communications for control, reinforcement learning, networked control systems and industrial IoT.

Wenjin Wang (Member, IEEE) received the Ph.D. degree in communication and information systems from Southeast University, Nanjing, China, in 2011. From 2010 to 2014, he was with the School of System Engineering, University of Reading, Reading, U.K. He is currently a Professor with the National Mobile Communications Research Laboratory, Southeast University. His research interests include advanced signal processing for future wireless communications and satellite communications. Dr. Wang was awarded the Best Paper Award from IEEE WCSP'09. He was also awarded the first grade Technological Invention Award of the State Education Ministry of China in 2009.

Shi Jin (Fellow, IEEE) received the B.S. degree in communications engineering from Guilin University of Electronic Technology, Guilin, China, in 1996, the M.S. degree from Nanjing University of Posts and Telecommunications, Nanjing, China, in 2003, and the Ph.D. degree in information and communications engineering from Southeast University, Nanjing, in 2007. From June 2007 to October 2009, he was a Research Fellow at the Adastral Park Research Campus, University College London, London, U.K. He is currently affiliated with the faculty of the National Mobile Communications Research Laboratory, Southeast University. His research interests include wireless communications, random matrix theory, and information theory. He serves as an Area Editor for the IEEE Transactions on Communications and IET Electronics Letters. He was previously an Associate Editor for the IEEE Transactions on Wireless Communications, IEEE Communications Letters, and IET Communications. Dr. Jin and his co-authors were awarded the 2011 IEEE Communications Society Stephen O. Rice Prize Paper Award in the field of communication theory, a 2022 Best Paper Award, and a 2010 Young Author Best Paper Award by the IEEE Signal Processing Society, and 2023 Jack Neubauer Memorial Award by the IEEE Vehicular Technology Society.

Vincent K. N. Lau (Fellow, IEEE) received the B.Eng. (Hons.) degree from The University of Hong Kong, in 1992, and the Ph.D. degree from Cambridge University in 1997. He was with Bell Labs from 1997 to 2004, and the Department of Electronic and Computer Engineering (ECE), The Hong Kong University of Science and Technology (HKUST), in 2004. Currently, he is the Chair Professor and the Founding Director of Huawei-HKUST Innovation Laboratory, HKUST. His research interests include robust and delay-optimal cross layer optimization for MIMO/OFDM wireless systems, interference mitigation techniques for wireless networks, massive MIMO, M2M, and network control systems.